

## (IN-)STABILITY AND STABILIZATION OF QNL-TYPE ATOMISTIC-TO-CONTINUUM COUPLING METHODS\*

CHRISTOPH ORTNER<sup>†</sup>, ALEXANDER V. SHAPEEV<sup>‡</sup>, AND LEI ZHANG<sup>§</sup>

**Abstract.** We study the stability of ghost force-free energy-based atomistic-to-continuum (a/c) coupling methods. In one dimension we essentially complete the theory by introducing a universally stable a/c coupling as well as a stabilization mechanism for unstable coupling schemes. We then present a comprehensive study of a two-dimensional scalar planar interface setting, as a step towards a general two-dimensional/three-dimensional vectorial analysis. Our results point out various new challenges. For example, we find that none of the ghost force-free methods known to us is universally stable (i.e., stable under general interaction and general loads). We then explore to what extent our one-dimensional stabilization mechanism can be extended.

**Key words.** atomistic-to-continuum coupling, quasicontinuum, stability

**AMS subject classifications.** 65Q99, 74S30, 65N12, 70C20

**DOI.** 10.1137/130933873

**1. Introduction.** Atomistic-to-continuum (a/c) coupling schemes are a class of computational multiscale methods for the efficient simulation of crystalline solids in the presence of defects. Different variants have been among the tools of computational materials science for many decades [18, 9, 19]. More recently, a numerical analysis theory of a/c coupling has emerged; we refer the reader to [17] for an introduction, a summary of the state of the art, and extensive references.

While the *consistency* theory of a/c coupling methods has a solid foundation [21, 23], understanding their stability properties essentially remains an outstanding open problem. The main difficulty is that the a/c model interface, even if treated consistently, can generate new eigenmodes present in neither the atomistic nor the continuum model, which can render a/c coupling methods unstable. Indeed, we emphasize that we are not only concerned with questions of analysis but also with the construction of stable schemes.

In one dimension, an essentially complete survey of stability is presented in the review article [17], which is partially based on the results of the present paper. In dimensions greater than one, very little is known. A universal stability result has been proven in [15], but for a coupling scheme that requires a macroscopically thick interface region. Some recent progress on getting sharp bounds on the required blending width for force-based a/c coupling [13, 14] remains incomplete and partially based on numerical evidence. For a sharp interface force-based coupling scheme more comprehensive analytical results are presented in [16], but even these are restricted to

---

\*Received by the editors August 21, 2013; accepted for publication (in revised form) May 12, 2014; published electronically September 9, 2014.

<http://www.siam.org/journals/mms/12-3/93387.html>

<sup>†</sup>Mathematics Institute, University of Warwick, Coventry CV4 7AL, UK (christoph.ortner@warwick.ac.uk). This author's research was supported by EPSRC grant EP/H003096 and ERC starting grant 335120.

<sup>‡</sup>School of Mathematics, University of Minnesota, Minneapolis, MN 55455 (ashapeev@math.umn.edu). This author's research was supported by AFOSR award FA9550-12-1-0187.

<sup>§</sup>Department of Mathematics, Institute of Natural Sciences, and MOE Key Lab in Scientific and Engineering Computing, Shanghai Jiao Tong University, Shanghai 200240, China (lzhang2012@sjtu.edu.cn). This author's research was supported by EPSRC grant EP/H003096 and the One Thousand Plan of China.

flat a/c interfaces and are dependent upon conditions that cannot be readily checked analytically.

In the present work we focus on the stability of a particular class of conservative a/c schemes, generally called coupling schemes of quasinonlocal (QNL) type. In one dimension we present examples of stability and instability (section 3), construct a new “universally stable” scheme (section 4), and further show how unstable QNL schemes can be stabilized (section 5).

We then consider a two-dimensional (2D) model problem, for which our results are more limited, in that we need to make much more stringent assumptions on the deformation and interaction potential than in one dimension. Within these assumptions, we show that there is a source of instability in 2D interfaces which was not present in the one-dimensional (1D) setting (section 7.1). Moreover, we show that this instability is universal. It is not only present in specific instances of QNL-type a/c couplings, but in a fairly wide class of generalized *geometric reconstruction* methods [25] (section 7.2), which cover most of the existing methods. This new source of instability is more severe than the instabilities observed in one dimension and cannot be “easily” stabilized. To be precise, we show that stabilizing QNL-type schemes in two dimensions severely affects their consistency when the system approaches a bifurcation point (section 7.4).

## 2. A general 1D QNL formulation.

**2.1. Notation for lattice functions.** For a lattice function  $v : \mathbb{Z} \rightarrow \mathbb{R}$  and  $\rho \in \mathbb{Z} \setminus \{0\}$ , we define the finite difference operators

$$D_\rho v(\xi) := v(\xi + \rho) - v(\xi).$$

For some finite interaction stencil  $\mathcal{R} = \{\pm 1, \dots, \pm r_{\text{cut}}\}$ , where  $r_{\text{cut}} \in \mathbb{N}$  is a fixed cut-off radius, we define

$$Dv(\xi) := (D_\rho v(\xi))_{\rho \in \mathcal{R}}.$$

The space of compact displacements is defined by

$$\mathcal{W}_0 := \{u : \mathbb{Z} \rightarrow \mathbb{R} \mid \text{supp}(u) \text{ is bounded}\}.$$

Each lattice function  $v : \mathbb{Z} \rightarrow \mathbb{R}$  is identified with its canonical continuous piecewise affine interpolant. In particular, we define the gradients  $\nabla v(x) := v(\xi) - v(\xi - 1)$  for  $x \in (\xi - 1, \xi)$ .

If  $H : \mathcal{W}_0 \rightarrow \mathcal{W}_0^*$  is a linear operator (or  $\langle H \cdot, \cdot \rangle$  a bilinear form on  $\mathcal{W}_0$ ), then we define the associated stability constant

$$\gamma(H) := \inf_{\substack{u \in \mathcal{W}_0 \\ \|\nabla u\|_{L^2} = 1}} \langle Hu, u \rangle.$$

We say that  $H$  is stable if  $\gamma(H) > 0$ .

**2.2. Many-body interactions for an infinite chain.** We consider finite range many-body interactions of deformed configurations of the infinite chain  $\mathbb{Z}$ . Let  $V \in C^2(\mathbb{R}^{\mathcal{R}})$  be the many-body site energy potential with partial derivatives

$$V_\rho(\mathbf{g}) := \frac{\partial V(\mathbf{g})}{\partial g_\rho} \quad \text{and} \quad V_{\rho\varsigma}(\mathbf{g}) := \frac{\partial^2 V(\mathbf{g})}{\partial g_\rho \partial g_\varsigma} \quad \text{for } \mathbf{g} = (g_\rho)_{\rho \in \mathcal{R}} \in \mathbb{R}^{\mathcal{R}}.$$

We assume that  $V$  is invariant under reflections of the local configuration, that is,

$$(2.1) \quad V((g_\rho)_{\rho \in \mathcal{R}}) = V((-g_{-\rho})_{\rho \in \mathcal{R}}).$$

Immediate consequences of (2.1) are the symmetries

$$(2.2) \quad V_{-\rho}(\mathbf{F}\mathcal{R}) = -V_\rho(\mathbf{F}\mathcal{R}) \quad \text{and} \quad V_{-\rho, -\varsigma}(\mathbf{F}\mathcal{R}) = V_{\rho\varsigma}(\mathbf{F}\mathcal{R}) \quad \forall \rho, \varsigma \in \mathcal{R}, \mathbf{F} > 0.$$

A macroscopic strain  $\mathbf{F}$  and a displacement  $u \in \mathcal{W}_0$  induce a deformed configuration  $y(\xi) = \mathbf{F}\xi + u(\xi)$ ,  $\xi \in \mathbb{Z}$ . To such a configuration we assign the energy difference

$$(2.3) \quad \mathcal{E}^a(y) := \sum_{\xi \in \mathbb{Z}} [V(Dy(\xi)) - V(\mathbf{F}\mathcal{R})].$$

Since the lattice sum is finite, this expression is well defined. The first and second variations with respect to  $u$  (in the sense of Gâteaux derivatives) are also well defined and are given by

$$\begin{aligned} \langle \delta \mathcal{E}^a(y), v \rangle &:= \sum_{\xi \in \mathbb{Z}} \sum_{\rho \in \mathcal{R}} V_\rho(Dy(\xi)) \cdot D_\rho v(\xi) \quad \text{and} \\ \langle \delta^2 \mathcal{E}^a(y)v, v \rangle &:= \sum_{\xi \in \mathbb{Z}} \sum_{\rho, \varsigma \in \mathcal{R}} V_{\rho\varsigma}(Dy(\xi)) \cdot D_\rho v(\xi) D_\varsigma v(\xi) \quad \text{for } v \in \mathcal{W}_0. \end{aligned}$$

We are particularly interested in the second variation evaluated at the homogeneous deformation  $y = \mathbf{F}x$  (where  $(\mathbf{F}x)(\xi) := \mathbf{F}\xi$ ),

$$(2.4) \quad \langle H_F^a v, v \rangle := \langle \delta^2 \mathcal{E}^a(\mathbf{F}x)v, v \rangle = \sum_{\xi \in \mathbb{Z}} \sum_{\rho, \varsigma \in \mathcal{R}} V_{\rho\varsigma} \cdot D_\rho v(\xi) D_\varsigma v(\xi),$$

where, here and throughout most of this paper, we are suppressing the dependence of  $V_{\rho\varsigma}$  on  $\mathbf{F}\mathcal{R}$  when it is clear from the context that we mean  $V_{\rho\varsigma}(\mathbf{F}\mathcal{R})$ .

The stability of nonhomogeneous states  $y = \mathbf{F}x + u$  can be deduced from the stability of homogeneous states; see [17, Theorem 7.8].

**2.3. A general QNL formulation.** The QNL approximation of  $\mathcal{E}^a$  [28] transitions between the atomistic model and a continuum model by introducing a modified site potential at the a/c interface. To simplify our analysis we focus on a single a/c interface. Let  $(-\infty, 0] \cap \mathbb{Z}$  be the atomistic region and  $\mathbb{R}_+ := (0, \infty)$  be the continuum region. In the atomistic region, we employ modified site energies  $\tilde{V}_\xi \in C^2(\mathbb{R}^{\mathcal{R}})$ ,  $\xi \leq 0$ , while in the continuum region we employ the Cauchy–Born strain energy density [1, 10, 8, 24],

$$W(\mathbf{G}) := V(\mathbf{G}\mathcal{R}).$$

The QNL a/c coupling energy functional is then given by

$$(2.5) \quad \mathcal{E}^{ac}(y) := \sum_{\xi=-\infty}^0 [\tilde{V}_\xi(Dy(\xi)) - V(\mathbf{F}\mathcal{R})] + \int_{1/2}^\infty [W(\nabla y) - W(\mathbf{F})] dx$$

for all deformations  $y = \mathbf{F}x + u$ ,  $u \in \mathcal{W}_0$ .

We shall assume throughout that the modified site energies satisfy the following conditions: there exists  $\xi_0 \in \mathbb{Z}_-$  such that

$$(2.6) \quad \tilde{V}_{\xi,\rho}(Dy(\xi)) = 0 \quad \text{whenever } \xi + \rho > 1,$$

$$(2.7) \quad \tilde{V}_\xi(Dy) = V(Dy) \quad \text{for } \xi \leq \xi_0,$$

$$(2.8) \quad \delta \mathcal{E}^{\text{ac}}(\mathbf{F}x) = 0 \quad \forall \mathbf{F} > 0.$$

Condition (2.6) states that atoms do not interact with the continuum region, except for the interface atom at  $\xi = 0$ . Condition (2.7) states that the transition region is bounded. Condition (2.8) is the force-consistency condition (absence of “ghost forces”), which ensures first-order consistency of the QNL approximation [21].

As in the case of the atomistic model,  $\mathcal{E}^{\text{ac}}$  is well defined and has variations in the sense of Gâteaux derivatives. The second variation, evaluated at the homogeneous deformation  $y = \mathbf{F}x$ ,  $H_{\mathbf{F}}^{\text{ac}} = \delta^2 \mathcal{E}^{\text{ac}}(\mathbf{F}x)$ , is given by

$$(2.9) \quad \langle H_{\mathbf{F}}^{\text{ac}} u, u \rangle = \sum_{\xi=-\infty}^0 \sum_{\rho, \varsigma \in \mathcal{R}} \tilde{V}_{\xi,\rho\varsigma} \cdot D_\rho u(\xi) D_\varsigma u(\xi) + W''(\mathbf{F}) \int_{1/2}^\infty |\nabla u|^2 dx.$$

**2.3.1. Error in critical strains.** We shall be interested in understanding the regimes of strains  $\mathbf{F}$  for which  $H_{\mathbf{F}}^{\text{a}}$  and  $H_{\mathbf{F}}^{\text{ac}}$  are stable. To explain why this is relevant in practical simulations, consider the following description of a quasi-static loading scenario (adapted from [5]):

- (i)  $\mathbf{F}(t) \in C([t_0, t_*])$  is a given path in deformation space, where  $t_*$  is a critical load, and constants  $c_0, c_1 > 0$  such that

$$c_0(t_* - t) \leq \gamma(H_{\mathbf{F}(t)}^{\text{a}}) \leq c_1(t_* - t) \quad \text{for } t_0 \leq t \leq t_*.$$

At the critical load  $t_*$  (e.g., a bifurcation) an instability occurs, which typically indicates the onset of defect nucleation or defect motion (“critical event”).

- (ii) Suppose now that QNL is initially stable but has a reduced stability region:  $\gamma(H_{\mathbf{F}(t_0)}^{\text{qnl}}) > 0$  but  $\gamma(H_{\mathbf{F}(t_*)}^{\text{qnl}}) < 0$ . Then there exists a reduced critical load  $t_*^{\text{qnl}} < t_*$  such that  $\gamma(H_{\mathbf{F}(t_*^{\text{qnl}})}^{\text{qnl}}) = 0$ .

In such a situation we first of all predict an incorrect critical load, i.e., incorrect magnitude applied forces under which the critical event occurs. Moreover, since the event may occur in a different region of deformation space, it is even possible that a qualitatively different event is observed (e.g., a different type of defect is nucleated).

**2.3.2. Preliminary estimates.** We can immediately make the following generic observation.

**PROPOSITION 2.1.**  $\gamma(H_{\mathbf{F}}^{\text{ac}}) \leq \gamma(H_{\mathbf{F}}^{\text{a}})$  for all  $\mathbf{F} > 0$ .

*Remark 2.2.* If the atomistic region is finite, then we would obtain that  $\gamma(H_{\mathbf{G}}^{\text{ac}}) \leq \gamma(H_{\mathbf{F}}^{\text{a}}) + \text{err}$ , where err decreases with increasing atomistic region size. See [10] for results along these lines.

*Proof.* Let  $\varepsilon > 0$ , and let  $u \in \mathcal{W}_0$  such that  $\|\nabla u\|_{L^2} = 1$  and  $\langle H_{\mathbf{F}}^{\text{a}} u, u \rangle \leq \gamma(H_{\mathbf{F}}^{\text{a}}) + \varepsilon$ . Upon shifting  $u$  by  $v(\xi) = u(\xi + \eta)$  for  $\eta$  sufficiently large, we can assume without loss of generality that  $u(\xi) = 0$  for all  $\xi \geq \xi_0 - r_{\text{cut}} - 1$ . Therefore, we obtain

$$\gamma(H_{\mathbf{F}}^{\text{ac}}) \leq \langle H_{\mathbf{F}}^{\text{ac}} u, u \rangle = \langle H_{\mathbf{F}}^{\text{a}} u, u \rangle \leq \gamma(H_{\mathbf{F}}^{\text{a}}) + \varepsilon.$$

Since  $\varepsilon$  was arbitrary, the result follows.  $\square$

Proposition 2.1 ensures that if a lattice  $\mathbf{F}\mathbb{Z}$  is unstable in the atomistic model, then it must also be unstable in the a/c coupling model. The converse question, whether stability of  $H_{\mathbf{F}}^a$  implies stability of  $H_{\mathbf{F}}^{ac}$ , is more difficult to answer in general. This question was first raised in [5] for 1D second-neighbor Lennard-Jones-type pair interactions, where this implication holds. Further investigations in this direction can be found in [6, 12, 11]. In the present paper we aim to present a more complete picture for the case of general range many-body interactions.

To conclude this section, we present another elementary auxiliary result that we will reference later on. Let the Cauchy–Born energy functional be given by  $\mathcal{E}^c(y) := \int_{\mathbb{R}} [W(\nabla y) - W(\mathbf{F})] dx$  and the corresponding hessian operator by

$$\langle H_{\mathbf{F}}^c u, u \rangle := W''(\mathbf{F}) \|\nabla u\|_{L^2}^2.$$

Then we have the following result.

LEMMA 2.3.  $\gamma(H_{\mathbf{F}}^c) = W''(\mathbf{F}) \geq \gamma(H_{\mathbf{F}}^a)$  for all  $\mathbf{F} > 0$ .

*Proof.* The idea of this result is classical; see, for example, [29]. A proof, which can be translated verbatim to our present setting, is given in [10].  $\square$

### 3. (In-)stability of a second-neighbor QNL method.

**3.1. The second-neighbor QNL method.** The original QNL energy, in the case of second neighbors ( $\mathcal{R} = \{\pm 1, \pm 2\}$ ), is given by [28, 4]

$$(3.1) \quad \begin{aligned} \mathcal{E}^{\text{qnl}}(y) = & \sum_{\xi=-\infty}^{-2} [V(Dy(\xi)) - V(\mathbf{F}\mathcal{R})] + \sum_{\xi=-1}^0 [V(\tilde{D}y(\xi)) - V(\mathbf{F}\mathcal{R})] \\ & + \int_{1/2}^{\infty} [W(\nabla y) - W(\mathbf{F})] dx, \end{aligned}$$

where

$$\tilde{D} := (D_{-2}, D_{-1}, D_1, 2D_1).$$

(That is, interaction of interface atoms with the atomistic region uses the atomistic finite difference,  $D_{-j}$ , while interaction of interface atoms with the continuum region uses only the nearest-neighbor finite difference,  $jD_1$ .)

It is well known that this energy functional is force consistent [28, 7],

$$\langle \delta \mathcal{E}^{\text{qnl}}(\mathbf{F}x), v \rangle = 0 \quad \forall v \in \mathcal{W}_0,$$

which implies a general first-order consistency result [17, 21].

Moreover, for the case of Lennard-Jones-type interactions under expansion, and periodic boundary conditions, it has been shown in [5] that  $\gamma(H_{\mathbf{F}}^{\text{qnl}}) > 0$  if and only if  $\gamma(H_{\mathbf{F}}^a) > 0$ , up to a small error. This can be generalized and translated to our setting as follows.

PROPOSITION 3.1. *Suppose that  $\mathcal{R} = \{\pm 1, \pm 2\}$  and  $V(Dy) = \sum_{j \in \mathcal{R}} \phi(|D_j y|)$ , where  $\phi \in C^2(\mathbb{R}_+)$ . Then, for  $\mathbf{F} > 0$ ,  $\gamma(H_{\mathbf{F}}^{\text{qnl}}) > 0$  if and only if  $\gamma(H_{\mathbf{F}}^a) > 0$ .*

*Proof.* We give only a brief outline of the proof, as the essential ideas are already contained in [5].

We already know that  $\gamma(H_{\mathbf{F}}^{\text{qnl}}) \leq \gamma(H_{\mathbf{F}}^a)$ , and hence we prove only the opposite inequality.

A short calculation (see [5, 17] for more details), employing the identity

$$\phi''(2F)|D_2u(\xi)|^2 = 2\phi''(2F)\{|D_1u(\xi)|^2 + |D_1u(\xi+1)|^2\} - \phi''(2F)|D_1^2u(\xi)|^2,$$

yields

$$(3.2) \quad \langle H^{\text{qnl}}u, u \rangle = \langle H^cu, u \rangle - \phi''(2F) \sum_{\xi=-\infty}^{-2} |D_1^2u(\xi)|^2.$$

Hence, if  $\phi''(2F) \leq 0$  (Lennard-Jones case), then  $\gamma(H_F^{\text{qnl}}) \geq \gamma(H_F^c) \geq \gamma(H_F^a)$ .

If  $\phi''(2F) > 0$ , then employing the identity  $\langle H^au, u \rangle = \langle H^cu, u \rangle - \phi''(2F)\|D_1^2u\|_{\ell^2}^2$  (which follows from the same calculation as (3.2)), we obtain

$$\langle H^{\text{qnl}}u, u \rangle = \langle H^au, u \rangle + \phi''(2F) \sum_{\xi=-1}^{\infty} |D_1^2u(\xi)|^2.$$

Hence,  $\gamma(H_F^{\text{qnl}}) \geq \gamma(H_F^a)$ .  $\square$

**3.2. Instability example.** Proposition 3.1 leads us to investigate whether the result holds also for general many-body interactions. An analysis of Li and Luskin [11] in a similar context, but ignoring the transition from the a/c model, indicates that this may be false. Indeed, we can construct a counterexample. Here, we present only a brief summary but give more detail in section A.1. Our example is somewhat academic in that we do not show that any concrete interaction potential exhibits this instability, but only that it may occur *in principle*.

For ease of notation, we write  $V_{\rho,\varsigma} = V_{\rho,\varsigma}(F\mathcal{R})$ . Exploiting the point symmetry of  $V$ , possibly rescaling by a scalar, we assume that

$$\begin{aligned} V_{1,1} &= V_{-1,-1} = 1, & V_{1,-1} &=: \alpha, \\ V_{2,2} &= V_{-2,-2} =: \beta, & V_{2,-2} &=: \gamma, \\ V_{1,2} &= V_{-1,-2} = -V_{-1,2} = -V_{1,-2} =: \delta \end{aligned}$$

for parameters  $\alpha, \beta, \gamma, \delta \in \mathbb{R}$ . The additional symmetry  $V_{1,2} = -V_{-1,2}$  that we employed is consistent with EAM-type potentials.

With these parameters, and a lengthy computation following [5, 11], we obtain

$$(3.3) \quad \begin{aligned} \langle H_F^{\text{qnl}}u, u \rangle &= A \sum_{\xi \in \mathbb{Z}} |D_1u(\xi)|^2 + \sum_{\xi=-\infty}^{-0} B_\xi |D_1^2u(\xi)|^2 \\ &\quad + \sum_{\xi=-\infty}^{-1} C_\xi |D_1^3u(\xi)|^2 + D \sum_{\xi=-\infty}^{-2} |D_1^4u(\xi)|^2, \end{aligned}$$

where  $A, B_\xi, C_\xi, D \in \mathbb{R}$  are coefficients that depend linearly on the parameters  $\alpha, \beta, \gamma, \delta$ .

Choosing the parameter values  $\alpha = -0.99$ ,  $\beta = 0.1$ ,  $\gamma = 0.15$ ,  $\delta = -0.2$  yields

$$\begin{aligned} A &= 0.38; \\ B_0 &= 0.91, \quad B_{-1} = 3.26, \quad B_{-2} = 3.56, \quad B_\xi = 3.91 \quad \text{for } \xi \leq -3; \\ C_{-1} &= -0.5, \quad C_{-2} = -1.3, \quad C_\xi = -1.6 \quad \text{for } \xi \leq -3; \\ D &= 0.15. \end{aligned}$$

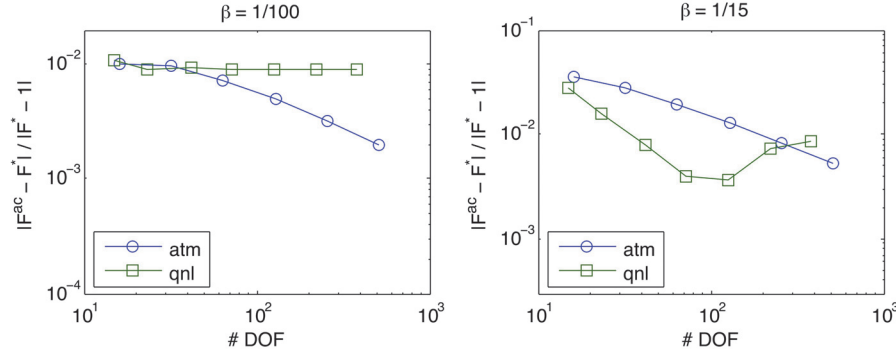


FIG. 1. Relative errors of critical strains for QNL and the restricted atomistic simulation. The external forces are parameterized by  $\alpha = 1.5$ ,  $\beta \in \{0.01, 0.066\}$ . See section A.2 for details of the model and the computation.

By a numerical calculation, we obtain that

$$\gamma(H_F^{\text{qnl}}) < -0.005.$$

Conversely, using straightforward Fourier analysis, we can show that

$$\gamma(H_F^{\text{a}}) = 0.02.$$

That is,  $H_F^{\text{a}}$  is stable, while  $H_F^{\text{qnl}}$  is unstable with this choice of parameters. The details of the calculation are given in section A.1.

**3.3. A numerical example.** The counterexample from section 3.2 is somewhat dissatisfying in that it is based purely on experimenting with coefficients, but there is no clear connection to a physical problem of interest where the predicted discrepancy in stability occurs. We therefore present a numerical example of a 1D chain with EAM-type interaction and applied external forces, for which we can still observe this stability gap. We give a brief outline of the experiment setup; the details of the model and of the setup are given in section A.2.

We reformulate the QNL model in a finite domain  $\{-N, \dots, N\}$  with atomistic region  $\{-K, \dots, K\}$ . This is implemented by applying the boundary condition  $y(\xi) = F\xi$  for  $|\xi| \geq N$ . Moreover, we apply an external force, to be able to observe nonlinear deformation effects. Finally, we discretize the continuum region using P1 finite elements. Given  $N$ , the atomistic region size  $K$  and the FE mesh are chosen quasi-optimally.

We define the critical strain,  $F^{\text{qnl}}$ , to be the smallest strain greater than one, for which the corresponding equilibrium  $y_F$  of the energy is unstable, i.e.,  $\gamma(\delta^2 \mathcal{E}^{\text{qnl}}(y_F)) \leq 0$ .

The exact critical strain  $F^*$ , against which the error is measured, is defined to be the critical strain for the unrestricted atomistic model.

In Figure 1 we plot the relative errors in the critical strains, for increasing domain sizes and hence increasing computational cost (measured in terms of the number of degrees of freedom required for the computation), for the QNL method and for the restricted atomistic model. We observe that the critical strains in the restricted atomistic model display clear systematic convergence, whereas the critical strains of the QNL method appear to diverge or converge to a wrong limit.

**4. A universally stable a/c coupling in one dimension.** Motivated by the results of section 3 we seek a/c couplings with universally reliable stability properties.

DEFINITION 4.1. *An a/c coupling energy  $\mathcal{E}^{\text{ac}}$  is universally stable if, for all interaction potentials  $V \in C^2(\mathbb{R}^{\mathcal{R}})$  and strains  $\mathbf{F} > 0$ ,  $\gamma(H_{\mathbf{F}}^{\text{ac}}) > 0$  if and only if  $\gamma(H_{\mathbf{F}}^{\text{a}}) > 0$ .*

The analysis in [17] indicates that the behavior we observed in section 3.3 would not be possible if the QNL method were universally stable, and indeed we saw in section 3.2 that counterexamples can be constructed.

We will now present the construction of a universally stable a/c coupling. For simplicity, we consider again the case where the atomistic region is given by  $\mathbb{Z}_- = \{0, -1, -2, \dots\}$ . The *reflection method*, which we formulate in the following paragraphs, can be understood as a special case of the QNL and geometric reconstruction ideas [7, 25, 28] but with a particularly simple reconstruction operator.

For any lattice function  $z : \mathbb{Z} \rightarrow \mathbb{R}$  (both deformations and displacements) we denote its antisymmetric reflection about the origin by

$$z^* := \begin{cases} z(\xi), & \xi \leq 0, \\ 2z(0) - z(-\xi), & \xi > 0. \end{cases}$$

With this notation we define, for  $y = \mathbf{F}x + u, u \in \mathcal{W}_0$ ,

$$\begin{aligned} \mathcal{E}^{\text{rf}}(y) &:= \mathcal{E}^*(y) + \int_0^\infty W(\nabla y) \, dx, \quad \text{where} \\ \mathcal{E}^*(y) &:= \sum_{\xi=-\infty}^{-1} [V(Dy^*(\xi)) - V(\mathbf{F}\mathcal{R})] + \frac{1}{2} [V(Dy^*(0)) - V(\mathbf{F}\mathcal{R})]. \end{aligned}$$

One may readily check that  $\mathcal{E}^{\text{rf}}$  is of the general form (2.5).

The key property, the reason for the name “reflection method,” and in fact the motivation for the definition of  $\mathcal{E}^{\text{rf}}$ , is the following.

LEMMA 4.2. *Let  $y = \mathbf{F}x + u, u \in \mathcal{W}_0$ ; then  $\mathcal{E}^*(y) = \frac{1}{2}\mathcal{E}^{\text{a}}(y^*)$ .*

*Proof.* By definition,  $y^*$  is antisymmetric about the origin, and consequently,

$$\begin{aligned} D_\rho y^*(\xi) &= y^*(\xi + \rho) - y^*(\xi) \\ &= [2y^*(0) - y^*(-\xi - \rho)] - [2y^*(0) - y^*(-\xi)] \\ &= -D_{-\rho} y^*(-\xi). \end{aligned}$$

Due to the reflection symmetry (2.1) of  $V$ , we obtain  $V(Dy^*(\xi)) = V(Dy^*(-\xi))$ , which implies the stated result.  $\square$

THEOREM 4.3. *The a/c coupling  $\mathcal{E}^{\text{rf}}$  is force consistent,*

$$(4.1) \quad \langle \delta \mathcal{E}^{\text{rf}}(\mathbf{F}x), v \rangle = 0,$$

*and universally stable,*

$$(4.2) \quad \gamma(H_{\mathbf{F}}^{\text{rf}}) = \gamma(H_{\mathbf{F}}^{\text{a}}).$$

*Proof of (4.1).* From Lemma 4.2 we obtain

$$\langle \delta \mathcal{E}^*(\mathbf{F}x), v \rangle = \frac{1}{2} \langle \delta \mathcal{E}^{\text{a}}(\mathbf{F}x), v^* \rangle,$$



where we note that  $v^*$  does not necessarily belong to  $\mathcal{W}_0$ , but  $\nabla v^*$  has compact support and hence the right-hand side is well defined. Lemma 12 in [21] implies that

$$(4.3) \quad \langle \delta \mathcal{E}^a(Fx), v^* \rangle = W'(F) \int_{\mathbb{R}} \nabla v^*(x) dx.$$

(Note that [21, Lemma 12] is in fact a 2D result; however, the 1D variant is proven verbatim using the 1D bond density formula [26, Proposition 3.3]. Alternatively, (4.3) can be proven directly from [26, Proposition 3.1].)

Since  $\nabla v^*$  is symmetric about the origin, (4.3) implies that

$$\langle \delta \mathcal{E}^*(F), v \rangle = \frac{1}{2} W'(F) \int_{\mathbb{R}} \nabla v^*(x) dx = W'(F) \int_{-\infty}^0 \nabla v(x) dx = W'(F) v(0).$$

Inserting this into the definition of  $\delta \mathcal{E}^{\text{rf}}$ , we obtain

$$\langle \delta \mathcal{E}^{\text{rf}}(F), v \rangle = W'(F) v(0) + \int_0^\infty W'(F) \nabla v(x) dx = 0.$$

*Proof of (4.2).* Applying again Lemma 4.2, as well as the symmetry of  $\nabla v^*$ , we obtain

$$\begin{aligned} \langle H_F^{\text{rf}} v, v \rangle &= \langle \delta^2 \mathcal{E}^*(F) v, v \rangle + W''(F) \int_0^\infty |\nabla v|^2 dx \\ &= \frac{1}{2} \langle \delta^2 \mathcal{E}^a(Fx) v^*, v^* \rangle + W''(F) \|\nabla v\|_{L^2(0,\infty)}^2 \\ &\geq \frac{1}{2} \gamma(H_F^a) \|\nabla v^*\|_{L^2(\mathbb{R})}^2 + \gamma(H_F^c) \|\nabla v\|_{L^2(0,\infty)}^2 \\ &= \gamma(H_F^a) \|\nabla v\|_{L^2(-\infty,0)}^2 + \gamma(H_F^c) \|\nabla v\|_{L^2(0,\infty)}^2 \geq \gamma(H_F^a) \|\nabla v\|_{L^2(\mathbb{R})}^2; \end{aligned}$$

that is,  $\gamma(H_F^{\text{rf}}) \geq \gamma(H_F^a)$ . Proposition 2.1 shows that this inequality is in fact an equality.  $\square$

## 5. Stabilizing the 1D QNL method.

**5.1. The general strain gradient representation.** A key component in previous sharp stability analyses of a/c methods was a decomposition of a/c Hessians into the Cauchy–Born Hessian and a strain gradient correction [5, 20, 12]. Here we generalize these representations to general many-body finite range interactions.

LEMMA 5.1. *For  $\xi \in \mathbb{Z}, \rho \in \mathcal{R}$ , define the sets*

$$A(\xi, \rho) := \begin{cases} \{\xi, \dots, \xi + \rho - 1\}, & \rho > 0, \\ \{\xi + \rho, \dots, \xi - 1\}, & \rho < 0. \end{cases}$$

*Then, for  $\xi \in \mathbb{Z}, \rho, \varsigma \in \mathcal{R}$ ,*

$$D_\rho u(\xi) D_\varsigma u(\xi) = \frac{\rho \varsigma}{2|\rho||\varsigma|} \sum_{\eta \in A(\xi, \rho)} \sum_{\eta' \in A(\xi, \varsigma)} \{|D_1 u(\eta)|^2 + |D_1 u(\eta')|^2 - |D_1 u(\eta) - D_1 u(\eta')|^2\}.$$

*Proof.* It is clear from the definitions that

$$D_\rho u(\xi) = \frac{\rho}{|\rho|} \sum_{\eta \in A(\xi, \rho)} D_1 u(\eta),$$

and therefore,

$$D_\rho u(\xi) D_\varsigma u(\xi) = \frac{\rho\varsigma}{|\rho||\varsigma|} \sum_{\eta \in A(\xi, \rho)} \sum_{\eta' \in A(\xi, \varsigma)} D_1 u(\eta) D_1 u(\eta').$$

Applying the identity

$$D_1 u(\eta) D_1 u(\eta') = \frac{1}{2} |D_1 u(\eta)|^2 + \frac{1}{2} |D_1 u(\eta')|^2 - \frac{1}{2} |D_1 u(\eta) - D_1 u(\eta')|^2$$

yields the stated result.  $\square$

LEMMA 5.2. *Let  $H_F^{\text{ac}}$  be of the general form (2.9); then*

$$(5.1) \quad \langle H_F^{\text{ac}} u, u \rangle = \langle H_F^{\text{e}} u, u \rangle + \langle \Delta_F^{\text{ac}} u, u \rangle,$$

where

$$(5.2) \quad \langle \Delta_F^{\text{ac}} u, u \rangle = \sum_{j=1}^{2r_{\text{cut}}-1} \sum_{\xi=-\infty}^0 c_j(\xi) |D_1 u(\xi) - D_1 u(\xi - j)|^2 \quad \text{with}$$

$$c_j(\xi) = \sum_{\rho, \varsigma \in \mathcal{R}} \frac{\rho\varsigma}{2|\rho||\varsigma|} \sum_{\substack{\eta \in \mathbb{Z}_- \\ \xi \in A(\eta, \rho), \xi-j \in A(\eta, \varsigma)}} \tilde{V}_{\eta, \rho\varsigma}(\mathcal{FR}).$$

*Proof.* Applying Lemma 5.1 to the representation (2.9) of the QNL hessian, we immediately obtain that

$$(5.3) \quad \langle H_F^{\text{ac}} u, u \rangle = \sum_{\xi \in \mathbb{Z}} c_0(\xi) |D_1 u(\xi)|^2 + \langle \Delta_F^{\text{ac}} u, u \rangle,$$

where  $\Delta_F^{\text{ac}}$  is of the form (5.2), and  $c_0(\xi) \in \mathbb{R}$  are some coefficients that still need to be determined. The stated identity for  $c_j(\xi)$ ,  $j \geq 1$ , in the definition of the strain gradient operator  $\Delta_F^{\text{ac}}$  follows from a straightforward exchange of summation.

To determine  $c_0(\xi)$ , we first note that (2.6) implies  $c_0(\xi) = W''(\mathbf{F})$  for  $\xi \geq 1$ .

To determine the remaining coefficients we apply the force-consistency condition (2.8). We know from (2.8) that

$$\langle \delta \mathcal{E}^{\text{ac}}((\mathbf{F} + t\mathbf{G})x), v \rangle = 0 \quad \forall v \in \mathcal{W}_0,$$

for all  $\mathbf{F} > 0$ ,  $\mathbf{G} \in \mathbb{R}$ , and  $t$  sufficiently small. Taking the derivative with respect to  $t$ , evaluated at  $t = 0$ , yields

$$\langle \delta^2 \mathcal{E}^{\text{ac}}(\mathbf{F}x) \mathbf{G}x, v \rangle = 0 \quad \forall v \in \mathcal{W}_0,$$

or, written in terms of the representation (5.3),

$$\sum_{\xi \in \mathbb{Z}} c_0(\xi) (\mathbf{G} \cdot a_1) D_1 v(\xi) + \langle \Delta_F^{\text{ac}} \mathbf{G}x, v \rangle = 0,$$

where we extended the definition of  $c_0(\xi)$  by  $c_0(\xi) = W''(\mathbf{F})$  for  $\xi > 0$ .

Since  $\mathbf{G}x$  is an affine function,  $\langle \Delta_F^{\text{ac}} \mathbf{G}x, v \rangle = 0$ , and hence we obtain that

$$\sum_{\xi \in \mathbb{Z}} c_0(\xi) D_1 v(\xi) = 0 \quad \forall v \in \mathcal{W}_0.$$

This implies  $\xi \mapsto c_0(\xi)$  must be a constant, and in particular,  $c_0(\xi) \equiv W''(\mathbf{F})$ .  $\square$

**5.2. The stabilized QNL method.** We observed in Lemma 5.2 that the QNL hessian can be written as the Cauchy–Born hessian with a strain gradient correction in the atomistic and interface region. Moreover, due to the “bounded interface condition” (2.7), we know that the strain gradient correction is the same for the QNL and for the reflection Hessians, except in a bounded neighborhood of the interface. More precisely, we can write

$$(5.4) \quad \langle H_F^{\text{qnl}} u, u \rangle = \langle H_F^{\text{rfl}} u, u \rangle + \langle (\Delta_F^{\text{qnl}} - \Delta_F^{\text{rfl}}) u, u \rangle,$$

where

$$\langle (\Delta_F^{\text{qnl}} - \Delta_F^{\text{rfl}}) u, u \rangle = \sum_{j=1}^{2r_{\text{cut}}-1} \sum_{\xi=\xi_1}^{-1} c'_j(\xi) |D_1 u(\xi) - D_1 u(\xi - j)|^2$$

for some  $\xi_1 \leq 0$  that depends on  $\xi_0$  and on  $r_{\text{cut}}$  and for coefficients  $c'_j(\xi) := c_j(\xi) - c_j^{\text{rfl}}(\xi)$ . If  $c'_j(\xi) \geq 0$  for all  $\xi$ , then we obtain that  $\langle H_F^{\text{qnl}} u, u \rangle \geq \langle H_F^{\text{rfl}} u, u \rangle$ , and hence the QNL method is universally stable.

If  $c'_j(\xi) < 0$  for some  $j, \xi$ , then we can redefine a *stabilized QNL energy*

$$(5.5) \quad \mathcal{E}^{\text{stab}}(y) := \mathcal{E}^{\text{qnl}}(y) + \kappa \langle Su, u \rangle \quad \text{for } y = Fx + u, u \in \mathcal{W}_0,$$

where  $\kappa > 0$  is a stabilization constant and  $S$  is the stabilization operator defined through

$$(5.6) \quad \langle Su, u \rangle := \sum_{\xi=\xi_1-2r_{\text{cut}}+2}^{-1} |D_{-1} D_1 u(\xi)|^2.$$

Because the stabilization involves only second derivatives, this modification does not affect the first-order consistency of the QNL method; see Remark 5.4.

**THEOREM 5.3.** *Fix a bounded set  $\mathcal{F} \subset \mathbb{R}$  (a range of macroscopic strains  $F$  of interest). Then there exists a constant  $\kappa_0 \geq 0$  such that, for all  $\kappa \geq \kappa_0$  and for all  $F \in \mathcal{F}$ ,  $\delta^2 \mathcal{E}^{\text{stab}}(Fx)$  is stable if and only if  $H_F^{\text{a}}$  is stable.*

An upper bound on  $\kappa_0$  is given by

$$\kappa_0 \leq \sup_{F \in \mathcal{F}} \sum_{\rho, \varsigma \in \mathcal{R}} (|\rho| + |\varsigma|)^2 |\rho| |\varsigma| \sup_{\xi \in \mathbb{Z}_-} |V_{\xi, \rho\varsigma}(F\mathcal{R}) - V_{\xi, \rho\varsigma}(F)|,$$

where  $V_{\xi}^{\text{rfl}}$  is the effective site potential of the reflection scheme.

*Proof.* We know from Proposition 2.1 that if  $H_F^{\text{a}}$  is unstable, then  $H_F^{\text{stab}}$  is unstable, so we need only prove the converse statement.

Since the reflection method is universally stable, it follows from (5.4) that it is sufficient to prove that

$$\langle (\Delta_F^{\text{qnl}} - \Delta_F^{\text{rfl}}) u, u \rangle + \kappa \langle Su, u \rangle \geq 0$$

for  $\kappa$  sufficiently large. To prove that this is indeed the case, we simply compute an upper bound on  $|\langle (\Delta_F^{\text{qnl}} - \Delta_F^{\text{rfl}}) u, u \rangle|$ :

$$\begin{aligned} |\langle (\Delta_F^{\text{qnl}} - \Delta_F^{\text{rfl}}) u, u \rangle| &\leq \sum_{j=1}^{2r_{\text{cut}}-1} \sum_{\xi=\xi_1}^{-1} |c'_j(\xi)| |D_1 u(\xi) - D_1 u(\xi - j)|^2 \\ &\leq \sum_{j=1}^{2r_{\text{cut}}-1} \sum_{\xi=\xi_1}^{-1} |c'_j(\xi)| j \sum_{\eta=\xi-j+1}^{\xi} |D_{-1} D_1 u(\eta)|^2, \end{aligned}$$

where we used the Cauchy–Schwarz (or the Jensen) inequality. Upon reordering the summation, we obtain

$$\begin{aligned} & |(\Delta_F^{\text{qnl}} - \Delta_F^{\text{rfl}})u, u| \\ & \leq \sum_{\eta=\xi_1-2r_{\text{cut}}+2}^{-1} |D_{-1}D_1u(\eta)|^2 \left\{ \sum_{j=\max(1, \xi_1-\eta+1)}^{2r_{\text{cut}}-1} \sum_{\xi=\max(\eta, \xi_1)}^{\min(\eta+j-1, -1)} |c'_j(\xi)|j \right\} \\ & =: \sum_{\eta=\xi_1-2r_{\text{cut}}+2}^{-1} |D_{-1}D_1u(\eta)|^2 d'(\mathbf{F}, \eta). \end{aligned}$$

Letting  $\kappa_0 := \max_{\eta, \mathbf{F} \in \mathcal{F}} d'(\mathbf{F}, \eta)$  yields the result.

To get an upper bound on this quantity, we next estimate  $|c'_j(\xi)|$ . Let

$$m'(\rho, \varsigma) := \sup_{\xi \in \mathbb{Z}_-} \sup_{\mathbf{F} \in \mathcal{F}} |V_{\xi, \rho\varsigma} - V_{\xi, \rho\varsigma}^{\text{rfl}}|;$$

then

$$|c'_j(\xi)| \leq \frac{1}{2} \sum_{\rho, \varsigma \in \mathcal{R}} \sum_{\substack{\eta \in \mathbb{Z}_- \\ \xi \in A(\eta, \rho), \xi-j \in A(\eta, \varsigma)}} m'(\rho, \varsigma),$$

and noting that the sum over  $\eta$  is taken over at most  $\min(|\rho|, |\varsigma|)$  sites and, moreover, that only the sum over  $\rho, \varsigma$  satisfying  $|\rho| + |\varsigma| \geq j$  needs to be taken into account, we obtain

$$|c'_j(\xi)| \leq \frac{1}{2} \sum_{\substack{\rho, \varsigma \in \mathcal{R} \\ |\rho|+|\varsigma| \geq j}} \min(|\rho|, |\varsigma|) m'(\rho, \varsigma).$$

Inserting this estimate into the definition of  $d'(\mathbf{F}, \eta)$  gives

$$d'(\mathbf{F}, \eta) \leq \sum_{j=\max(1, \xi_1-\eta+1)}^{2r_{\text{cut}}-1} \sum_{\xi=\max(\eta, \xi_1)}^{\min(\eta+j-1, -1)} \sum_{\substack{\rho, \varsigma \in \mathcal{R} \\ |\rho|+|\varsigma| \geq j}} \frac{1}{2} \min(|\rho|, |\varsigma|) (|\rho| + |\varsigma|) m'(\rho, \varsigma),$$

where we estimated  $j \leq (|\rho| + |\varsigma|)$ . Next, using  $\frac{1}{2} \min(|\rho|, |\varsigma|) (|\rho| + |\varsigma|) \leq |\rho||\varsigma|$ , and noting that the sum over  $\xi$  ranges over at most  $j$  values, we further estimate

$$\begin{aligned} d'(\mathbf{F}, \eta) & \leq \sum_{j=\max(1, \xi_1-\eta+1)}^{2r_{\text{cut}}-1} j \sum_{|\rho|+|\varsigma| \geq j} |\rho||\varsigma| m'(\rho, \varsigma) \\ & \leq \sum_{\rho, \varsigma \in \mathcal{R}} |\rho||\varsigma| m'(\rho, \varsigma) \sum_{j=1}^{\min(2r_{\text{cut}}-1, |\rho|+|\varsigma|)} j \leq \sum_{\rho, \varsigma \in \mathcal{R}} |\rho||\varsigma| (|\rho| + |\varsigma|)^2 m'(\rho, \varsigma). \end{aligned}$$

This establishes the estimate for  $\kappa_0$ .  $\square$

*Remark 5.4* (consistency of the stabilized QNL method). If the cost of stabilizing the QNL method is a loss in consistency, then little can be gained by the procedure proposed in the foregoing section. However (ignoring finite element coarsening of the continuum region), it is easy to show that

$$\|\delta \mathcal{E}^{\text{stab}}(u) - \delta \mathcal{E}^{\text{a}}(u)\|_{\mathcal{W}^*} \leq \|\delta \mathcal{E}^{\text{qnl}}(u) - \delta \mathcal{E}^{\text{a}}(u)\|_{\mathcal{W}^*} + 2\kappa_0 \|D_{-1}D_1u\|_{\ell^2(\mathcal{I})},$$

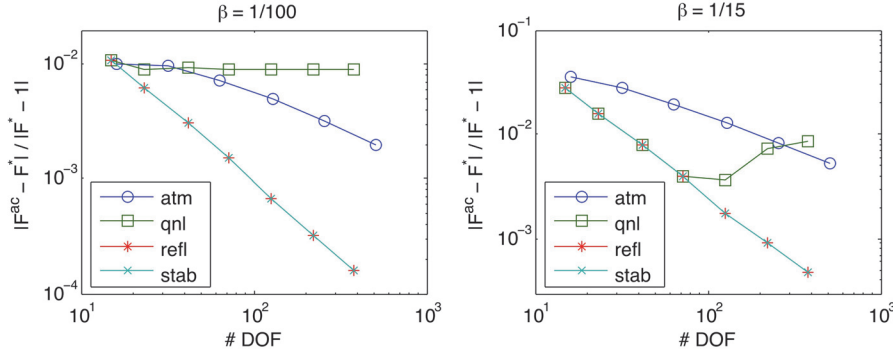


FIG. 2. Relative errors of critical strains for the QNL, REFL, and stabilized QNL methods and external forces parameterized by  $\alpha = 1.5$ ,  $\beta \in \{0.01, 0.066\}$ . The stabilization parameter for the stabilized QNL method is  $\kappa = 0.1$ . The graphs for the REFL and STAB methods lie visually on top of one another.

where  $\mathcal{I} := \{\xi_1 - 2r_{\text{cut}} + 1, \dots, -1\}$ . That is, the additional consistency error committed by the stabilization is of first order, which is the same as the consistency error of the QNL method [20, 21, 25, 2]. (The terminology for the *order* of the upper bound follows the convention used in [17].)

Moreover, the prefactor  $\kappa_0$  is bounded in terms of the partial derivatives  $V_{\xi, \rho_\varsigma}$ . Having some uniform bound on these partial derivatives  $V_{\xi, \rho_\varsigma}$  is a prerequisite to obtain a first-order error estimate [21, 25]. For example, for geometric reconstruction-type methods [28, 7, 25] one can show that these are bounded in terms of a norm on the reconstruction coefficients.

In summary, we can conclude that the stabilization (5.4) will normally not affect the consistency of the QNL method.

**5.3. Numerical example.** We may now revisit the numerical example from section 3.3 and add the universally stable reflection method and the stabilized QNL method to the graph. We choose the QNL stabilization parameter  $\kappa = 0.1$  by trial and error. The extension of the two methods to the finite domain used in this experiment is straightforward.

The result is displayed in Figure 2. We observe clear systematic convergence of the critical strains for both the reflection method and the stabilized QNL method, which is consistent with our analysis in the foregoing sections.

**6. QNL formulation of a 2D nearest-neighbor scalar model.** In the remainder of the paper we explore possible generalizations of our foregoing results to higher dimensions. We are unable, at present, to provide results of the same generality as in one dimension, and we therefore restrict our presentation to the setting of nearest-neighbor many-body interactions for scalar displacement fields (e.g., antiplane displacements) in two dimensions, with a “flat” a/c interface. Already in this simple setting, we will encounter several difficult new issues that must be overcome before focusing on the even more challenging vectorial case and general interface geometries. (For the majority of our results, admitting a wider interaction range does not cause major additional difficulties; see, in particular, [22, Appendix A.4].)

**6.1. Notation for the 2D triangular lattice.** Our 2D analysis is most convenient to perform in the setting of the 2D triangular lattice, which we denote by

$$\Lambda := \mathbb{A}\mathbb{Z}^2, \quad \text{where} \quad \mathbb{A} = \begin{pmatrix} 1 & \cos(\pi/3) \\ 0 & \sin(\pi/3) \end{pmatrix}.$$

For future reference, we define the six nearest-neighbor lattice directions by  $a_1 := (1, 0)$ , and  $a_j := \mathbb{Q}_6^{j-1} a_1$ ,  $j \in \mathbb{Z}$ , where  $\mathbb{Q}_6$  denotes the rotation through angle  $2\pi/6$  and we note that  $a_{j+3} = -a_j$ .

For a lattice function  $w : \Lambda \rightarrow \mathbb{R}$ , we define the nearest-neighbor differences

$$D_j w(\xi) := w(\xi + a_j) - w(\xi).$$

The interaction range is defined as  $\mathcal{R} = \{a_1, \dots, a_6\}$  and the corresponding finite difference stencil as  $Dw(\xi) = \{D_j w(\xi)\}_{j=1}^6$ . Let  $\|Dw\|_{\ell^2} := (\sum_{\xi \in \Lambda} \sum_{j=1}^6 |D_j w(\xi)|^2)^{1/2}$ .

Let  $\mathcal{T}$  denote the canonical triangulation of  $\mathbb{R}^2$  with nodes  $\Lambda$ , using *closed* triangles; then each lattice function  $v$  is identified with its continuous piecewise affine interpolant with respect to  $\mathcal{T}$ . In particular, we define  $\nabla v_T$  to be the gradient of  $v$  in  $T \in \mathcal{T}$  and we note that  $\nabla v_T \cdot a_j = D_j v(\xi)$  if  $\xi, \xi + a_j \in T$ .

The space of admissible test functions is again the space of compactly supported lattice functions, defined by

$$\mathcal{W}_0 := \{u : \Lambda \rightarrow \mathbb{R} \mid \text{supp}(u) \text{ is bounded}\}.$$

For an operator  $H : \mathcal{W}_0 \rightarrow \mathcal{W}_0^*$  we define again  $\gamma(H) := \inf_{u \in \mathcal{W}_0, \|\nabla u\|_{L^2} = 1} \langle Hu, u \rangle$ .

**6.2. 2D many-body nearest-neighbor interactions.** We fix a nearest-neighbor many-body (i.e., 7-body) potential  $V \in C^2(\mathbb{R}^6)$ , with partial derivatives

$$V_i(\mathbf{g}) = \frac{\partial V(\mathbf{g})}{\partial g_i} \quad \text{and} \quad V_{ij}(\mathbf{g}) = \frac{\partial^2 V(\mathbf{g})}{\partial g_i \partial g_j} \quad \text{for } \mathbf{g} = (g_i)_{i=1}^6 \in \mathbb{R}^6.$$

For a deformed configuration  $y = \mathbb{F} \cdot x + u$  (where  $x(\xi) = \xi$  and  $\mathbb{F} \in \mathbb{R}^2$ ) we define the energy difference by

$$(6.1) \quad \mathcal{E}^a(y) = \sum_{\xi \in \Lambda} [V(Dy(\xi)) - V(\mathbb{F}\mathcal{R})].$$

Since the sum is effectively finite,  $\mathcal{E}^a$  is well defined and admits two variations in the sense of Gâteaux derivatives, with the second variation given by

$$\langle \delta^2 \mathcal{E}^a(y) v, v \rangle = \sum_{\xi \in \Lambda} \sum_{i,j=1}^6 V_{ij}(Dy(\xi)) \cdot D_i v(\xi) D_j v(\xi).$$

We are again particularly interested in homogeneous states  $y(x) = \mathbb{F}x$ , and we define

$$(6.2) \quad \langle H_{\mathbb{F}}^a u, u \rangle = \sum_{\xi \in \Lambda} \sum_{i,j=1}^6 V_{ij} \cdot D_i u(\xi) D_j u(\xi),$$

where, here and throughout, we omit the argument  $\mathbb{F}\mathcal{R}$  in  $V_{ij}$  when it is clear from the context that we mean  $V_{ij}(\mathbb{F}\mathcal{R})$ .

**6.2.1. Symmetries.** Inversion symmetry about each lattice point leads us to assume that  $V((g_i)_{i=1}^6) = V((-g_{i'})_{i=1}^6)$ , where  $i' \in \{1, \dots, 6\}$  such that  $a_{i'} = -a_i$ . This yields the point symmetry for the second derivatives  $V_{i,j}(\mathcal{FR}) = V_{i',j'}(\mathcal{FR})$  for  $i, j \in \{1, \dots, 6\}$ ; see, e.g., [24]. Since the reference lattice  $\Lambda$  has full hexagonal symmetry, it is reasonable to make the stronger assumption that  $V$  has full hexagonal symmetry as well, i.e.,

$$(6.3) \quad V(\mathbf{g}) = V(g_6, g_1, \dots, g_5).$$

In this case, but only for the deformation  $\mathbf{F} = \mathbf{0}$ , one can readily deduce the identities

$$(6.4) \quad \begin{aligned} V_{1,1} &= \dots = V_{6,6} =: \alpha_0, \\ V_{1,2} &= \dots = V_{5,6} = V_{6,1} =: \alpha_1, \\ V_{1,3} &= \dots = V_{4,6} = V_{5,1} = V_{6,2} =: \alpha_2, \\ V_{1,4} &= V_{2,5} = V_{3,6} =: \alpha_3, \end{aligned}$$

where  $V_{i,j} = V_{i,j}(\mathbf{0})$  and  $\alpha_i \in \mathbb{R}$ .

Both symmetries can be derived, e.g., by reducing a three-dimensional (3D) model to a scalar 2D antiplane model.

**6.3. QNL-type methods.** We define the Cauchy–Born approximation in a discrete sense,

$$\mathcal{E}^c(y) := \frac{1}{2} \sum_{T \in \mathcal{T}} [W(\nabla y_T) - W(\mathbf{F})],$$

where  $W(\mathbf{F}) := V(\mathcal{FR})$ . Unusually, we have not normalized  $W$  with respect to volume, which somewhat simplifies notation. (Since each site has associated volume 1, each element has associated volume  $3/6 = 1/2$ .)

We define the atomistic and continuum lattice sites

$$\Lambda^a := \{\xi \in \Lambda \mid \xi_2 < 0\}, \quad \Lambda^c := \{\xi \in \Lambda \mid \xi_2 > 0\},$$

and in addition the  $k$ th “row” of atoms

$$\Lambda^{(k)} := \{\xi \in \Lambda \mid \xi_2 = k\sqrt{3}/2\},$$

so that  $\Lambda^{(0)}$  is the set of interface lattice sites.

QNL methods are a/c coupling schemes with an energy functional of the form

$$(6.5) \quad \begin{aligned} E^{\text{qnl}}(y) &:= \sum_{\xi \in \Lambda^a} [V(Dy(\xi)) - V(\mathcal{FR})] + \sum_{\xi \in \Lambda^{(0)}} [\tilde{V}(Dy(\xi)) - V(\mathcal{FR})] \\ &\quad + \sum_{\xi \in \Lambda^c} \frac{1}{6} \sum_{T \in \mathcal{T}, \xi \in T} [W(\nabla y_T) - W(\mathbf{F})], \end{aligned}$$

where  $\tilde{V}$  is a modified interaction potential that is chosen to transition between the atomistic and Cauchy–Born descriptions. For more details we refer the reader to [28, 7, 21], and in particular [25], which is closest in terms of analytical setting and notation to our present paper.

We assume throughout that  $\tilde{V} \in C^2(\mathbb{R}^6)$ ; then the QNL energy is well defined for  $y = \mathbf{F} \cdot x + u$ ,  $u \in \mathcal{W}_0$  and has two variations in the sense of Gâteaux derivatives.

We assume that  $\mathcal{E}^{\text{qnl}}$  does not exhibit ghost forces,

$$(6.6) \quad \langle \delta \mathcal{E}^{\text{qnl}}(\mathbf{F}x), v \rangle = 0 \quad \forall v \in \mathcal{W}_0, \mathbf{F} \in \mathbb{R}^2,$$

and is *energy consistent*,

$$(6.7) \quad \tilde{V}(\mathbf{F}\mathcal{R}) = V(\mathbf{F}\mathcal{R}) \quad \forall \mathbf{F} \in \mathbb{R}^2.$$

Sometimes, to achieve a more compact notation, we write

$$\mathcal{E}^{\text{qnl}}(y) = \sum_{\xi \in \Lambda^a \cup \Lambda^{(0)}} [\tilde{V}_\xi(Dy(\xi)) - V(\mathbf{F}\mathcal{R})] + \sum_{T \in \mathcal{T}} w_T [W(\nabla y_T) - W(\mathbf{F})],$$

where  $\tilde{V}_\xi = \tilde{V}$  for  $\xi \in \Lambda^{(0)}$ ,  $\tilde{V}_\xi = V$  for  $\xi \in \Lambda^a$ , and  $w_T = \#(\Lambda^c \cap T)/6$ . The second variation (hessian) at  $y = \mathbf{F}x$ ,  $H_{\mathbf{F}}^{\text{qnl}} = \delta^2 \mathcal{E}^{\text{qnl}}(\mathbf{F}x)$ , is then given by

$$(6.8) \quad \langle H_{\mathbf{F}}^{\text{qnl}} u, u \rangle = \sum_{\xi \in \Lambda^a \cup \Lambda^{(0)}} \sum_{i,j=1}^6 \tilde{V}_{\xi,ij} \cdot D_i u(\xi) D_j u(\xi) + \sum_{T \in \mathcal{T}} w_T (\nabla u_T)^\top W''(\mathbf{F}) \nabla u_T,$$

where  $W''(\mathbf{F}) \in \mathbb{R}^{2 \times 2}$  is the hessian of  $W$ .

As in the foregoing 1D results we shall focus exclusively on stability at homogeneous states. We show in [22, Appendix A.6] how one may extend such results to the stability of nonhomogeneous states including defects.

We remark that the 2D variant of Lemma 2.3,  $\gamma(H_{\mathbf{F}}^a) \leq \gamma(H_{\mathbf{F}}^c)$ , remains true [10].

To illustrate that we are not talking about abstract methods, but concrete practical formulations, we now introduce three specific variants.

**6.3.1. The QCE method.** The simplest QNL variant is the QCE method [19, 3], which is defined by simply taking  $\tilde{V} = V$ . It is shown in [25] that in our present setting (nearest-neighbor interaction, flat interface) it satisfies the force-consistency condition (6.6).

We denote the resulting energy functional by  $\mathcal{E}^{\text{qce}}$ .

**6.3.2. The GRAC-2/3 method.** The QCE method does *not* satisfy the force-consistency condition (6.6) in domains with corners, nor for second-neighbor interactions [27, 28, 7, 3, 25], and it is still an open problem to formulate a general scheme that does. A class of methods has been introduced in [25], extending ideas in [28, 7], which in our context can be defined through

$$\tilde{V}(Dy) := V(\tilde{D}y), \quad \text{where} \quad \tilde{D}_i y := \lambda_i D_{i-1} y + (1 - \lambda_i) D_i y + \lambda_i D_{i+1} y$$

for  $\lambda_i \in \mathbb{R}$ . It is shown in [25] that, for flat interfaces, all of these schemes satisfy (6.6), and for the choice

$$\lambda_i = \begin{cases} 1/3, & i = 2, 3, \\ 0, & i = 1, 4, 5, 6 \end{cases}$$

(and only for this choice), the resulting method (GRAC-2/3) can be extended to domains with corners while still satisfying (6.6). We denote the resulting energy functional by  $\mathcal{E}^{\text{g23}}$ .



**6.3.3. The local reflection method.** Finally, we introduce a new a/c coupling scheme, inspired by our 1D reflection method.

The idea is to apply the reflection method on each site  $\xi \in \Lambda^{(0)}$ , by point reflection of the relevant finite difference, which amounts to defining

$$\tilde{D}_i := \begin{cases} D_i, & i = 1, 4, 5, 6, \\ -D_{i+3}, & i = 2, 3, \end{cases} \quad \text{and} \quad \tilde{V}(Dy) := \frac{1}{2}V(\tilde{D}y) + \frac{1}{6} \sum_{\substack{T \in \mathcal{T}^c \\ \xi \in T}} W(\nabla y_T),$$

where  $\mathcal{T}^c := \{T \in \mathcal{T} \mid x_2 \geq 0 \text{ for all } x \in T\}$ .

The idea can be seen more clearly if we write the resulting energy functional in the form

$$\begin{aligned} \mathcal{E}^{\text{lrf}}(y) &:= \sum_{\xi \in \Lambda^a} [V(Dy(\xi)) - V(FR)] + \frac{1}{2} \sum_{\xi \in \Lambda^{(0)}} [V(\tilde{D}y(\xi)) - V(FR)] \\ &\quad + \frac{1}{2} \sum_{T \in \mathcal{T}^c} [W(\nabla y_T) - W(F)]. \end{aligned}$$

It is straightforward to check that this method exhibits no ghost forces.

**6.4. Atomistic and Cauchy–Born hessian representations.** Our aim is to develop a generalization of our 1D hessian representation, Lemma 5.2. Towards this end, we first establish representations for the atomistic and Cauchy–Born Hessians. The result for the QNL hessian will be presented in section 7.

We first state two auxiliary lemmas. The first provides a mechanism for establishing whether two symmetric bilinear forms are equal.

LEMMA 6.1. *Let  $H_1, H_2$  be self-adjoint operators defined through*

$$\langle H_i u, u \rangle = \sum_{\xi \in \Lambda} \sum_{j=1}^3 h_{i,j}(\xi) |D_j u(\xi)|^2;$$

*then  $H_1 = H_2$  if and only if  $h_{1,j}(\xi) = h_{2,j}(\xi)$  for all  $\xi \in \Lambda$ ,  $j = 1, \dots, 3$ .*

*Proof.* For some  $\eta \in \Lambda$  and  $j \in \{1, 2, 3\}$ , we define  $u(\xi) = \delta_{\xi, \eta}$  and  $v(\xi) = \delta_{\xi, \eta + a_j}$ , where  $\delta$  is the Kronecker delta. Then the product  $D_k u(\xi) D_k v(\xi)$  is nonzero if and only if  $\xi = \eta$  and  $k = j$ . Hence,

$$0 = \langle (H_1 - H_2)u, v \rangle = -(h_{1,j}(\eta) - h_{2,j}(\eta)).$$

Hence we conclude that  $h_{1,j}(\eta) = h_{2,j}(\eta)$  for all  $\eta \in \Lambda$  and  $j = 1, 2, 3$ . The converse implication is trivial.  $\square$

In the “canonical” hessian representations of  $\mathcal{E}^a, \mathcal{E}^c, \mathcal{E}^{\text{qnl}}$ , products of finite differences  $D_i u(\xi) D_j u(\xi)$  occur; see (6.2) and (6.8). In one dimension, we converted these products into squares of strains and strain gradients. The next lemma provides an analogous representation for general mixed differences. In [22, Appendix A.4] we provide the generalization for general finite range interaction.

LEMMA 6.2. *Let  $u \in \mathcal{W}_0$ ,  $\xi \in \Lambda$ , and  $i \in \{1, \dots, 6\}$ ; then*

$$(6.9) \quad D_i u(\xi) D_{i+1} u(\xi) = \frac{1}{2} |D_i u(\xi)|^2 + \frac{1}{2} |D_{i+1} u(\xi)|^2 - \frac{1}{2} |D_{i+2} u(\xi + a_i)|^2,$$

$$(6.10) \quad \begin{aligned} D_i u(\xi) D_{i+2} u(\xi) &= \frac{1}{2} |D_{i+1} u(\xi)|^2 - \frac{1}{2} |D_{i+2} u(\xi + a_i)|^2 \\ &\quad - \frac{1}{2} |D_{i+3} u(\xi + a_{i+1})|^2 + \frac{1}{2} |D_i D_{i+2} u(\xi)|^2, \end{aligned}$$

$$(6.11) \quad D_i u(\xi) D_{i+3} u(\xi) = -\frac{1}{2} |D_i u(\xi)|^2 - \frac{1}{2} |D_{i+3} u(\xi)|^2 + \frac{1}{2} |D_{i+3} D_i u(\xi)|^2.$$

*Proof.* All three identities are straightforward to verify by direct calculations.  $\square$

PROPOSITION 6.3 (Cauchy–Born Hessian). *There exist  $c_j = c_j(\mathbf{F})$ ,  $j = 1, 2, 3$ , such that*

$$\langle H_{\mathbf{F}}^c u, u \rangle = \sum_{j=1}^3 c_j \sum_{\xi \in \Lambda} |D_j u(\xi)|^2,$$

where  $W''(\mathbf{F}) = \frac{1}{2} \sum_{j=1}^3 c_j a_j \otimes a_j$ .

In the hexagonally symmetric case (6.4), we have  $c_1 = c_2 = c_3 =: c$ .

*Proof.* The result can be checked by a straightforward calculation. The complete proof is given in [22, Appendix A.3].  $\square$

Next, we establish the “strain gradient” representation of the atomistic hessian. We define a *sum of squares*  $p : \mathbb{R}^K \rightarrow \mathbb{R}$  to be a diagonal homogeneous quadratic, i.e., a function of the form  $p(z) = \sum_{k=1}^K c_k z_k^2$ .

PROPOSITION 6.4. *There exists a sum of squares  $X = X_{\mathbf{F}} : \mathbb{R}^{36} \rightarrow \mathbb{R}$  such that*

$$\langle H_{\mathbf{F}}^a u, u \rangle = \langle H_{\mathbf{F}}^c u, u \rangle + \sum_{\xi \in \Lambda} X(D^2 u),$$

where  $D^2 u(\xi) = (D_i D_j u(\xi))_{i,j=1}^6$ .

*Proof.* Applying the identities (6.9)–(6.11) to the original form (6.2) of  $H_{\mathbf{F}}^a$ , and noting the translation invariance of these operations, we obtain

$$\langle H_{\mathbf{F}}^a u, u \rangle = \sum_{j=1}^3 c_j^a \sum_{\xi \in \Lambda} |D_j u(\xi)|^2 + \sum_{\xi \in \Lambda} X(D^2 u(\xi)),$$

where  $X(D^2 u) = \sum_{i,j} b_{ij} |D_i D_j u|^2$  for some coefficients  $b_{i,j} \in \mathbb{R}$ . All that remains is to show that  $c_j^a = c_j$  for  $j = 1, 2, 3$ .

To prove this, we use a scaling argument. Let  $u \in C_0^\infty(\mathbb{R}^2)$ , and let  $u^{(\varepsilon)}(\xi) := \varepsilon u(\varepsilon \xi)$ ; then it is elementary to show, treating the lattice sum as a quadrature rule (see [10, Proposition 2.1] for an analogous argument), that

$$\begin{aligned} \frac{2}{\sqrt{3}} \langle H_{\mathbf{F}}^c u^{(\varepsilon)}, u^{(\varepsilon)} \rangle &\rightarrow \int_{\mathbb{R}^2} \sum_{j=1}^3 c_j |\nabla u \cdot a_j|^2 dx = \int_{\mathbb{R}^2} (\nabla u)^\top \mathbf{C} \nabla u dx, \\ \frac{2}{\sqrt{3}} \langle H_{\mathbf{F}}^a u^{(\varepsilon)}, u^{(\varepsilon)} \rangle &\rightarrow \int_{\mathbb{R}^2} \sum_{j=1}^3 c_j^a |\nabla u \cdot a_j|^2 dx = \int_{\mathbb{R}^2} (\nabla u)^\top \mathbf{C}^a \nabla u dx, \end{aligned}$$

where  $\mathbf{C} = \sum_{j=1}^3 c_j a_j \otimes a_j$  and  $\mathbf{C}^a = \sum_{j=1}^3 c_j^a a_j \otimes a_j$ . (The factor  $2/\sqrt{3}$  accounts for the density of lattice sites.)

On the other hand, treating the original lattice sum (6.2) as a quadrature rule yields

$$\begin{aligned} \lim_{\varepsilon \rightarrow 0} \frac{2}{\sqrt{3}} \langle H_{\mathbf{F}}^a u^{(\varepsilon)}, u^{(\varepsilon)} \rangle &= \int_{\mathbb{R}^2} \sum_{i,j=1}^6 V_{ij}(\mathbf{F}\mathcal{R}) (\nabla u \cdot a_j) (\nabla u \cdot a_i) dx \\ &= \int_{\mathbb{R}^2} (\nabla u)^\top W''(\mathbf{F}\mathcal{R}) \nabla u dx, \end{aligned}$$

which coincides with  $\lim_{\varepsilon \rightarrow 0} \frac{2}{\sqrt{3}} \langle H_{\mathbf{F}}^c u^{(\varepsilon)}, u^{(\varepsilon)} \rangle$ . This is possible only if  $W''(\mathbf{F}\mathcal{R}) = \mathbf{C} = \mathbf{C}^a$ . Since the three rank-1 matrices  $a_j \otimes a_j$ ,  $j = 1, 2, 3$ , are linearly independent, we can conclude that  $c_j = c_j^a$  for  $j = 1, 2, 3$ .  $\square$

**6.5. Simple cases.** 1. Suppose that the potential  $V$  is such that  $V_{i,i+2} = V_{i,i+3} \equiv 0$  for all  $i = 1, \dots, 6$ ; that is, only the “neighboring bonds” interact. (In the hexagonally symmetric case, this amounts to assuming that  $\alpha_2 = \alpha_3 = 0$ .) This could, for example, be understood as a simple case of bond-angle interaction. Then, in the proof of Proposition 6.4, only the identity (6.9) is employed but neither (6.10) nor (6.11). Therefore,  $X \equiv 0$ , and we obtain that  $H_F^a = H_F^c$ .

2. In the hexagonally symmetric case (6.4), without assuming  $\alpha_2 = \alpha_3 = 0$ , a straightforward explicit computation yields

$$(6.12) \quad c = 2(\alpha_0 + \alpha_1 - \alpha_2 - \alpha_3),$$

$$X(D^2u) = \sum_{i=1}^6 (\alpha_2 |D_{i+2}D_i u|^2 + \alpha_3 |D_{i+3}D_i u|^2).$$

**7. Instability and stabilization in two dimensions.** In this section we will derive the “strain gradient” representation of the QNL hessian. We shall find that, in contrast to our 1D result (Lemma 5.2), in two dimensions there is a source of instability that is different from an error in the strain gradient coefficients and therefore more severe.

**7.1. QNL hessian representation.** Applying the rules (6.9)–(6.11) to the “canonical” QNL hessian representation (6.8) we obtain the following result.

**PROPOSITION 7.1.** *There exist coefficients  $\tilde{c}_j(\xi) = \tilde{c}_j(F, \xi)$  and sums of squares  $\tilde{X}_\xi : \mathbb{R}^{36} \rightarrow \mathbb{R}$  such that*

$$(7.1) \quad \langle H_F^{\text{qnl}} u, u \rangle = \sum_{j=1}^3 \sum_{\xi \in \Lambda} \tilde{c}_j(\xi) |D_j u(\xi)|^2 + \sum_{\xi \in \Lambda} \tilde{X}_\xi(D^2 u(\xi)).$$

Moreover, the following identities hold:

$$(7.2) \quad \tilde{c}_j(\xi) = c_j \quad \text{except if both } \xi, \xi + a_j \in \Lambda^{(-1)} \cup \Lambda^{(0)} \cup \Lambda^{(1)},$$

$$(7.3) \quad \tilde{X}_\xi = 0 \quad \text{for } \xi_2 > 0, \quad \text{and}$$

$$(7.4) \quad \tilde{X}_\xi = X \quad \text{for } \xi_2 < 0.$$

*Proof.* Applying the identities (6.9)–(6.11) to the hessian representation (6.8) we obtain (7.1), and all that remains is to prove (7.2)–(7.4).

The identities (7.3) and (7.4) follow from (i) the fact that the site potential of  $H_F^{\text{qnl}}$  coincides with that of  $H_F^a$  for  $\xi_2 < 0$  and  $H_F^c$  for  $\xi_2 > 0$ , and (ii) the fact that the sum of squares that the operations (6.9)–(6.11) create depends only on a site potential  $\tilde{V}_\xi$ .

The remaining property (7.2) can be obtained by understanding which bond coefficients  $c_i(\eta)$  are “influenced” by the operations (6.9)–(6.11) applied with a given center atom  $\xi$ . These are depicted in Figure 3, and after combining the graphs for the three identities and rotating them, we see that a lattice site  $\xi$  influences only the coefficients  $c_i(\eta)$  corresponding to the 12 bonds  $D_j u(\xi)$ ,  $j = 1, \dots, 6$ , and  $D_{j+2} u(\xi + a_j)$ ,  $j = 1, \dots, 6$ ; cf. Figure 4(a). From this, it follows that a given coefficient  $c_i(\eta)$  is influenced only by the four nodes of the two neighboring triangles; cf. Figure 4(b). Thus, only the bonds depicted in Figure 4(c) are affected by the modified site potentials, which are precisely those bonds contained in the strip  $\{x \in \mathbb{R}^2 \mid -\sqrt{3}/2 \leq x_2 \leq \sqrt{3}/2\}$ .  $\square$

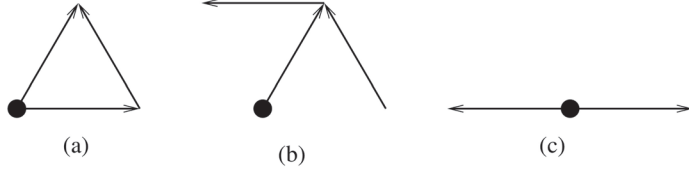


FIG. 3. Visualization of the identities (6.9)–(6.11). The bullets denote the sites  $\xi$ , while the arrows denote the terms  $|D_j u(\eta)|^2$  occurring in these identities. (a) visualizes (6.9); (b) visualizes (6.10); (c) visualizes (6.11).

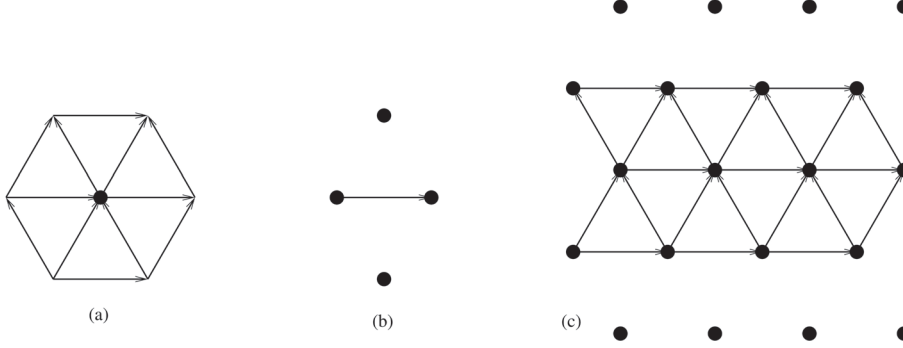


FIG. 4. (a) Bonds (arrows) that are affected by the operations (6.9)–(6.11) from a single site  $\xi$  (black disk); (b) sites (black disks) that affect a given bond (arrow) through the operations (6.9)–(6.11); (c) bonds for which the coefficients  $\tilde{c}_j(\xi)$  of the a/c hessian differ from the coefficients  $c_j$  of the Cauchy–Born hessian; cf. Proposition 7.1.

Although we have always restricted our presentation to the flat interface situation, all results up to this point are *generic*. That is, they can be generalized to interfaces with corners and even to long range interactions.

In the next result, where we provide some characterization of the coefficients  $\tilde{c}_j(\xi)$  in the interface region, we exploit tangential translation invariance.

**LEMMA 7.2.** *Suppose that the modified site energies are tangentially translation invariant, i.e.,  $\tilde{V}_\xi = \tilde{V}_{\xi+a_1}$  for all  $\xi \in \Lambda^{(0)}$ . Then the coefficients in the strain gradient representation (7.1) satisfy*

$$(7.5) \quad \tilde{c}_j(\xi) = c_j \quad \forall \xi \in \Lambda, \quad j = 2, 3.$$

Moreover, for  $j = 1$  and  $\xi \in \Lambda^{(m)}$ ,  $m = -1, 0, 1$ , we have  $\tilde{c}_1(\xi) = \tilde{c}_1^{(m)}$  (tangential translation invariance) and

$$(7.6) \quad \sum_{m=-1}^1 \tilde{c}_1^{(m)} = 3c_1.$$

*Proof.* Properties of  $\tilde{c}_2, \tilde{c}_3$ : By the same argument as in the 1D case (cf. Lemma 5.2) we can prove that

$$(7.7) \quad \langle H_F^{\text{qnl}} Gx, u \rangle = 0 \quad \forall u \in \mathcal{W}_0.$$

We fix  $\xi \in \Lambda$  and test (7.7) with  $u(\eta) := \delta_{\xi, \eta}$  (i.e., a “hat function”) to obtain

$$\sum_{j=1}^3 \tilde{c}_j(\xi)(-G \cdot a_j) + \sum_{j=1}^3 \tilde{c}_j(\xi - a_j)(G \cdot a_j) = 0.$$

If we define  $c_{j+3}(\xi) := c_j(\xi - a_j)$  for  $j = 1, 2, 3$ , then this can equivalently be stated as

$$-\mathbf{G} \cdot \sum_{j=1}^6 \tilde{c}_j(\xi) a_j = 0.$$

Since this must hold for all  $\mathbf{G} \in \mathbb{R}^2$ , we deduce that

$$(7.8) \quad \sum_{j=1}^6 \tilde{c}_j(\xi) a_j = 0 \quad \forall \xi \in \Lambda.$$

Using that fact that  $a_{j+3} = -a_j$  and  $a_1 + a_3 + a_5 = 0$ , we deduce that (7.8) is equivalent to

$$(7.9) \quad \tilde{c}_1(\xi) - \tilde{c}_4(\xi) = \tilde{c}_3(\xi) - \tilde{c}_6(\xi) = \tilde{c}_5(\xi) - \tilde{c}_2(\xi) \quad \forall \xi \in \Lambda.$$

We now test (7.9) with  $\xi \in \Lambda^{(1)}$ . Due to the translation invariance of the modified site energies it follows that  $\tilde{c}_1(\xi) = \tilde{c}_4(\xi)$ . Moreover,  $\tilde{c}_3(\xi) = c_3$  and  $\tilde{c}_2(\xi) = c_2$ , which implies that

$$0 = c_3 - \tilde{c}_6(\xi) = \tilde{c}_5(\xi) - c_2.$$

This implies (7.5) for  $\xi \in \Lambda^{(0)}$ . Analogously, testing (7.9) with  $\xi \in \Lambda^{(-1)}$  gives (7.5) for  $\xi \in \Lambda^{(-1)}$ .

*Properties of  $\tilde{c}_1$ :* We are left to establish the statements concerning the coefficients  $\tilde{c}_1$ . Due to the translation invariance of the site potential it immediately follows that  $\tilde{c}_j(\xi) = \tilde{c}_j(\xi + a_1)$ , and hence we can write  $\tilde{c}_j(\xi) = \tilde{c}_j^{(m)}$  for  $\xi \in \Lambda^{(m)}$ ,  $m = -1, 0, 1$ .

Finally, (7.6) is a consequence of the energy consistency (6.7). If we allowed noncompact test functions (as, e.g., in a periodic setting), then we could take the second variation of  $\mathcal{E}^a(\mathbf{F}x) = \mathcal{E}^{\text{qnl}}(\mathbf{F}x)$  along the displacement  $u = \mathbf{G}x$  and obtain  $\langle H_{\mathbf{F}}^a \mathbf{G}x, \mathbf{G}x \rangle = \langle H_{\mathbf{F}}^{\text{qnl}} \mathbf{G}x, \mathbf{G}x \rangle$ , which would imply (7.6). However, in our case  $\mathbf{G}x \notin \mathcal{W}_0$ , which makes the proof of (7.6) more involved.

We start with noticing that the energy consistency implies

$$\sum_{i,j=1}^6 (\tilde{V}_{i,j} - V_{i,j}) D_i u(\xi) D_j u(\xi) = 0$$

for  $u = \mathbf{G}x$  and some  $\xi \in \Lambda^{(0)}$ . We then rewrite this using the rules (6.9)–(6.11) as

$$\sum_{i=1}^3 \sum_{\substack{\rho \in \Lambda \\ \rho, \rho+a_i \in \mathcal{R} \cup \{0\}}} (\tilde{c}_{i,\rho} - c_{i,\rho}) |D_i u(\xi + \rho)|^2 + \tilde{X}(D^2 u(\xi)) - X(D^2 u(\xi)) = 0$$

with some  $\tilde{c}_{i,\rho}$  and  $c_{i,\rho}$ . Next, we substitute  $u = \mathbf{G}x$  and use  $D^2(\mathbf{G}x) = 0$ :

$$(7.10) \quad \sum_{i=1}^3 \sum_{\substack{\rho \in \Lambda \\ \rho, \rho+a_i \in \mathcal{R} \cup \{0\}}} (\tilde{c}_{i,\rho} - c_{i,\rho}) |\mathbf{G}a_i|^2 = 0.$$

It remains to notice that, since  $\tilde{c}_i^{(m)}$  and  $c_i$  were constructed using the same rules as  $\tilde{c}_{i,\rho}$  and  $c_{i,\rho}$ , we have

$$\sum_{\substack{\rho \in \Lambda \\ \rho, \rho + a_i \in \mathcal{R} \cup \{0\}}} (\tilde{c}_{i,\rho} - c_{i,\rho}) = \sum_{m=-1}^1 (\tilde{c}_i^{(m)} - c_i) \quad (i = 1, 2, 3).$$

Substituting this into (7.10), and using that  $\tilde{c}_i^{(m)} = c_i^{(m)}$  for  $i = 2, 3$ , we get

$$\sum_{m=-1}^1 (\tilde{c}_1^{(m)} - c_1) |\mathbf{G}a_1|^2 = 0$$

for all  $\mathbf{G}$ , which immediately implies (7.6).  $\square$

We see that the key difference between one and two dimensions for the stability of homogeneous deformations is that the  $|D_j u|^2$  coefficients in the 1D case are identical to those in the Cauchy–Born model for force-consistent a/c couplings, while this need not be the case in two dimensions. As a first step to showing that this can lead to an instability in two dimensions, we establish another representation of  $H_F^{\text{qnl}}$ .

LEMMA 7.3. *Under the conditions of Lemma 7.2, we have*

$$(7.11) \quad \langle H_F^{\text{qnl}} u, u \rangle = \langle H_F^c u, u \rangle + 2(\tilde{c}_1^{(1)} - \tilde{c}_1^{(-1)}) \langle K_0 u, u \rangle + \sum_{\xi \in \Lambda} \hat{X}_\xi(D^2 u(\xi)),$$

where  $\hat{X}_\xi$  are quadratic forms of  $D^2 u$  (not necessarily sums of squares), with  $\hat{X}_\xi = 0$  for  $\xi \in \Lambda^c$ , and

$$\langle K_0 u, u \rangle := \sum_{\xi \in \Lambda^{(0)}} D_2 D_1 u(\xi) D_1 u(\xi).$$

*Proof.* From Lemma 7.2 we have

$$\begin{aligned} \langle H_F^{\text{qnl}} u, u \rangle - \langle H_F^c u, u \rangle &= \sum_{\xi \in \Lambda} \tilde{X}_\xi(D^2 u(\xi)) \\ &= (\tilde{c}_1^{(1)} - c_1) \sum_{\xi \in \Lambda^{(0)}} (|D_1 u(\xi + a_2)|^2 - |D_1 u(\xi)|^2) \\ &\quad + (\tilde{c}_1^{(-1)} - c_1) \sum_{\xi \in \Lambda^{(0)}} (|D_1 u(\xi + a_5)|^2 - |D_1 u(\xi)|^2) \\ &= (\tilde{c}_1^{(1)} - c_1) \sum_{\xi \in \Lambda^{(0)}} (D_1 u(\xi + a_2) - D_1 u(\xi))(D_1 u(\xi + a_2) + D_1 u(\xi)) \\ &\quad + (\tilde{c}_1^{(-1)} - c_1) \sum_{\xi \in \Lambda^{(0)}} (D_1 u(\xi + a_5) - D_1 u(\xi))(D_1 u(\xi + a_5) + D_1 u(\xi)) \\ &= (\tilde{c}_1^{(1)} - c_1) \sum_{\xi \in \Lambda^{(0)}} D_2 D_1 u(\xi) (2D_1 u(\xi) + D_2 D_1 u(\xi)) \\ &\quad + (\tilde{c}_1^{(-1)} - c_1) \sum_{\xi \in \Lambda^{(0)}} D_5 D_1 u(\xi) (2D_1 u(\xi) + D_5 D_1 u(\xi)) \\ &= (\tilde{c}_1^{(1)} - \tilde{c}_1^{(-1)}) \sum_{\xi \in \Lambda^{(0)}} D_2 D_1 u(\xi) D_1 u(\xi) \end{aligned}$$

$$-(\tilde{c}_1^{(-1)} - c_1) \sum_{\xi \in \Lambda^{(0)}} D_5 D_2 D_1 u(\xi) D_1 u(\xi) + \cdots,$$

where “ $\cdots$ ” stands for some sum of squares of  $D^2 u(\xi)$ .

Summation by parts,

$$\sum_{\xi \in \Lambda^{(0)}} D_5 D_2 D_1 u(\xi) D_1 u(\xi) = - \sum_{\xi \in \Lambda^{(0)}} D_5 D_2 u(\xi) D_4 D_1 u(\xi),$$

completes the proof.  $\square$

## 7.2. Nonexistence of a universally stable method in two dimensions.

Lemma 7.3 suggests that, unless  $\tilde{c}_1^{(1)} - \tilde{c}_1^{(-1)} = 0$ , there is a discrepancy between  $H_F^{\text{qnl}}$  and  $H_F^c$  that is not a quadratic in  $D^2 u$  (and, as will be shown in section 7.3, unavoidably leads to an instability). We next establish that in fact  $\tilde{c}_1^{(1)} - \tilde{c}_1^{(-1)} \neq 0$  for a large family of a/c schemes, which not only includes examples from section 6.3 but also all geometric reconstruction-type variants [7, 25]. Below, we also present explicit calculations for the three methods from section 6.3.

**PROPOSITION 7.4.** *Consider the following generalization of the geometric reconstruction a/c (GRAC) method [25]:*

$$(7.12) \quad \tilde{V}(\mathbf{g}) = \sum_{\ell=1}^L w_\ell V(\mathbf{C}_\ell \mathbf{g}),$$

where  $w_\ell \in \mathbb{R}$ ,  $w_\ell \neq 0$ , and  $\mathbf{C}_\ell \in \mathbb{R}^{6 \times 6}$  ( $\ell = 1, \dots, L$ ). Assume that it satisfies the force- and energy-consistency conditions (6.6), (6.7). Further, assume hexagonal symmetry (6.4) of  $V$ , with  $\alpha_2 = \alpha_3 = 0$ .

Then there exist  $p_0, p_1 \in \mathbb{R}$  (depending on  $w_\ell, \mathbf{C}_\ell$ ) such that  $p_0 - p_1 = 1$  and

$$\tilde{c}_1^{(1)} - \tilde{c}_1^{(-1)} = p_0 \alpha_0 + p_1 \alpha_1.$$

In particular, there exists no choice of method parameters  $w_\ell, \mathbf{C}_\ell$  such that  $\tilde{c}_1^{(1)} - \tilde{c}_1^{(-1)} = 0$  for all parameters  $(\alpha_0, \alpha_1)$ .

*Proof.* *Step 1 (reduction to a GRAC).* Consider a method with interface site potential

$$(7.13) \quad \tilde{\tilde{V}}(\mathbf{g}) := V(\mathbf{B}\mathbf{g}),$$

where  $\mathbf{B} := \sum_{\ell=1}^L w_\ell \mathbf{C}_\ell$ . We show that it is energy and force consistent and, moreover,  $\langle \delta^2 \tilde{\tilde{V}}(\mathbf{F}\mathcal{R})u, u \rangle - \langle \delta^2 \tilde{V}(\mathbf{F}\mathcal{R})u, u \rangle$  is a sum of squares of  $D^2 u$  (and hence  $\tilde{c}_1^{(1)} - \tilde{c}_1^{(-1)}$  is the same for both methods).

Indeed, substituting  $V(\mathbf{g}) = v_0 + \mathbf{f} \cdot \mathbf{g}$  into the energy consistency condition (6.7) yields

$$v_0 \left( \sum_{\ell=1}^L w_\ell - 1 \right) + \mathbf{f} \cdot (\mathbf{B}\mathbf{F}\mathcal{R} - \mathbf{F}\mathcal{R}) = 0 \quad \forall v_0 \in \mathbb{R}, \quad \forall \mathbf{f} \in \mathbb{R}^6, \quad \forall \mathbf{F} \in \mathbb{R}^2.$$

Hence we get  $\sum_{\ell=1}^L w_\ell = 1$  and  $\mathbf{B}\mathbf{F}\mathcal{R} = \mathbf{F}\mathcal{R}$  for all  $\mathbf{F}$ . These identities make it straightforward to verify the energy and force consistency of (7.13), given the energy and force consistency of (7.12).

Finally, to show that  $\langle (\delta^2 \tilde{V}(\mathcal{FR}) - \delta^2 \tilde{V}(\mathcal{FR}))u, u \rangle$  is a sum of squares of  $D^2u$ , compute

$$(7.14) \quad \delta^2 \tilde{V}(\mathcal{FR}) = \sum_{\ell=1}^L w_\ell \mathbf{C}_\ell^\top \mathbf{H} \mathbf{C}_\ell,$$

where  $\mathbf{H} := \delta^2 V(\mathcal{FR}) \in \mathbb{R}^{6 \times 6}$  is the hessian of  $V$ . We apply the identity

$$\begin{aligned} w_\ell \mathbf{C}_\ell^\top \mathbf{H} \mathbf{C}_\ell + w_j \mathbf{C}_j^\top \mathbf{H} \mathbf{C}_j &= (w_\ell + w_j) \left( \frac{w_\ell \mathbf{C}_\ell + w_j \mathbf{C}_j}{w_\ell + w_j} \right)^\top \mathbf{H} \left( \frac{w_\ell \mathbf{C}_\ell + w_j \mathbf{C}_j}{w_\ell + w_j} \right) \\ &\quad + \frac{w_j w_\ell}{w_\ell + w_j} (\mathbf{C}_\ell - \mathbf{C}_j)^\top \mathbf{H} (\mathbf{C}_\ell - \mathbf{C}_j) \end{aligned}$$

to (7.14)  $L - 1$  times, noticing that the finite difference operator  $(\mathbf{C}_\ell - \mathbf{C}_j)Du$  is zero on all affine functions and hence can be represented as a sum of second differences. As a result, we express  $\delta^2 \tilde{V}(\mathcal{FR})$  as  $\delta^2 \tilde{V}(\mathcal{FR})$  plus squares of second differences.

*Step 2 (proof for a GRAC).* It is now sufficient to establish this proposition for a simpler method (7.13). Using the rules (6.9)–(6.11), we can express

$$\tilde{c}_1^{(1)} - \tilde{c}_1^{(-1)} = -\frac{1}{3}(\alpha_0 + 4\alpha_1) + \tilde{V}_{1,3} + \tilde{V}_{2,3} + \tilde{V}_{2,4} - \tilde{V}_{4,6} - \tilde{V}_{5,6} - \tilde{V}_{5,1},$$

which implies linearity of  $\tilde{c}_1^{(1)} - \tilde{c}_1^{(-1)}$  with respect to  $\alpha_0$  and  $\alpha_1$ , that is,  $\tilde{c}_1^{(1)} - \tilde{c}_1^{(-1)} = p_0 \alpha_0 + p_1 \alpha_1$ .

To see that  $p_0 - p_1 = 1$ , choose coefficients  $\alpha_0 = 1$  and  $\alpha_1 = -1$ , i.e., so that  $p_0 - p_1 = \tilde{c}_1^{(1)} - \tilde{c}_1^{(-1)}$ . In this case the hessian of  $V$  is given by

$$(7.15) \quad \mathbf{H} = \delta^2 V(\mathcal{FR}) = \begin{pmatrix} -1 & 1 & 0 & 0 & 0 & 1 \\ 1 & -1 & 1 & 0 & 0 & 0 \\ 0 & 1 & -1 & 1 & 0 & 0 \\ 0 & 0 & 1 & -1 & 1 & 0 \\ 0 & 0 & 0 & 1 & -1 & 1 \\ 1 & 0 & 0 & 0 & 1 & -1 \end{pmatrix}$$

and  $\delta^2 \tilde{V} = \mathbf{B}^\top \mathbf{H} \mathbf{B}$ . Next, denote the column vectors of  $\mathbf{B}$  as  $b_i \in \mathbb{R}^6$  and hence express

$$\tilde{c}_1^{(1)} - \tilde{c}_1^{(-1)} = 1 + b_1^\top \mathbf{H} b_3 + b_2^\top \mathbf{H} b_3 + b_2^\top \mathbf{H} b_4 - b_4^\top \mathbf{H} b_6 - b_5^\top \mathbf{H} b_6 - b_5^\top \mathbf{H} b_1$$

(here we used  $\frac{1}{3}(\alpha_0 + 4\alpha_1) = -1$ ).

Energy consistency (6.7) implies  $\sum_{i=1}^6 (\mathbf{F} a_i) b_i = (\mathbf{F} a_j)_{j=1}^6$  (we refer the reader to [25] for details). Using this identity with  $\mathbf{F} = \frac{2}{3}(a_6 + a_1)^\top$  and with  $\mathbf{F} = \frac{2}{3}(a_2 + a_3)^\top$  allows one to express

$$\begin{aligned} b_1 &= b_3 + b_4 - b_6 + (1, 0, -1, -1, 0, 1)^\top, \\ b_2 &= b_5 + b_6 - b_3 + (0, 1, 1, 0, -1, -1)^\top. \end{aligned}$$

Substituting these expressions into  $\tilde{c}_1^{(1)} - \tilde{c}_1^{(-1)}$  yields, after all cancellations,

$$\tilde{c}_1^{(1)} - \tilde{c}_1^{(-1)} = 1 + (1, 0, -1, -1, 0, 1) \mathbf{H} (b_3 - b_5) + (0, 1, 1, 0, -1, -1) \mathbf{H} (b_3 + b_4),$$

which equals identically 1 once (7.15) is used.  $\square$

*Remark 7.5.* Suppose that (in some practical problem)  $\mathbf{F} = \mathbf{F}_0$  is fixed and given a priori.

1. One can then consider energy-consistent methods with ghost force correction, such as in [19] (i.e., methods that satisfy (6.6) only for  $\mathbf{F} = \mathbf{F}_0$ ). Since we do not



explicitly use force consistency (6.6) in the proof, Proposition 7.4 would also be valid for such methods.

2. Nevertheless, it is possible to precompute  $\tilde{c}_1^{(1)} - \tilde{c}_1^{(-1)}$  and subtract the term  $\frac{1}{2}(\tilde{c}_1^{(1)} - \tilde{c}_1^{(-1)})((g_2 - g_3)^2 - (g_5 - g_6)^2)$  from  $\tilde{V}(\mathbf{g})$ , thus correcting the error in  $\tilde{c}_i(\xi)$ . However, beyond the nearest-neighbor planar interface scalar setting (which yields an interesting analytical study but is uninteresting for actual applications), it may not be easy to precompute these coefficients, and the practicality of this approach is therefore questionable.

3. For the three concrete schemes we introduced in section 6.3, in the fully symmetric case with  $\alpha_2 = \alpha_3 = 0$ , we obtain the following formulas (see [22, Appendix A.3] for proofs):

$$\begin{aligned}\langle H^{\text{qce}}u, u \rangle &= \langle H^a u, u \rangle + \frac{\alpha_0 + 4\alpha_1}{3} \sum_{\xi \in \Lambda^{(0)}} \left( |D_1 u(\xi)|^2 - |D_1 u(\xi + a_2)|^2 \right), \\ \langle H^{\text{lrf}}u, u \rangle &= \langle H^a u, u \rangle - \alpha_1 \sum_{\xi \in \Lambda^{(0)}} \left( |D_1 u(\xi)|^2 - |D_1 u(\xi + a_5)|^2 \right) + \sum_{\xi \in \Lambda^{(0)}} X^{\text{lrf}}(D^2 u(\xi)), \\ \langle H^{\text{g23}}u, u \rangle &= \langle H^a u, u \rangle + (\alpha_0 + 2\alpha_1) \sum_{\xi \in \Lambda^{(0)}} \left( |D_1 u(\xi)|^2 - |D_1 u(\xi + a_2)|^2 \right) \\ &\quad + \sum_{\xi \in \Lambda^{(0)}} X^{\text{g23}}(D^2 u(\xi)).\end{aligned}$$

**7.3. Instability.** It is fairly straightforward to see that  $\gamma(K_0) = \gamma(-K_0) < 0$  (cf. (7.11)). In this section we will show that the strain gradient correction (third group in (7.11)) cannot improve this indefiniteness of  $K_0$ , which will immediately imply the instability result (Corollary 7.7).

The strain gradient correction is clearly bounded by an operator of the form

$$(7.16) \quad \langle Su, u \rangle := \sum_{\xi \in \Lambda^{(0)}} |D^2 u(\xi)|^2,$$

that is,  $|\hat{X}_\xi(D^2 u)| \leq C|D^2 u(\xi)|^2$ . We therefore consider generic operators of the form

$$(7.17) \quad \langle K_\kappa u, u \rangle := \langle K_0 u, u \rangle + \kappa \langle Su, u \rangle.$$

We will show that  $K_\kappa$  is indefinite, independent of the choice of  $\kappa$ , and hence independent of the form the strain gradient correction  $\hat{X}_\xi$  takes. Note that this result is also a preparation for our analysis of the 2D analogue of the stabilization (5.5).

**LEMMA 7.6.** *There exists a constant  $c > 0$  such that*

$$(7.18) \quad \inf_{\substack{u \in \mathcal{H}_0 \\ \|Du\|_{\ell^2} = 1}} \langle K_\kappa u, u \rangle =: \lambda_\kappa \leq -\frac{c}{(\kappa + 1)^2}.$$

*Proof.* To obtain this bound, we make a separation of variables ansatz,

$$u(\xi) = u(ma_1 + na_2) = \alpha_m \beta_n,$$

and we define  $\alpha'_m := \alpha_{m+1} - \alpha_m$ ,  $\alpha''_m := \alpha_{m+1} - 2\alpha_m + \alpha_{m-1}$ , and analogous notation for  $\beta$ .

Next, let  $A, B \in C^\infty(\mathbb{R})$  be compactly supported with  $B(0) = 1$ , and let  $B'(0) = 1$ ,  $B''(0) = 0$ .

Let  $N \in \mathbb{N}$ , and define  $\alpha_m := A(m/N)$  and  $\beta_n := B(n/N)$ ; then simple scaling arguments show that, for  $N \geq N_0$  (sufficiently large),

$$\begin{aligned} \beta'_0 &\approx N^{-1}, & |\beta''_0| &\lesssim N^{-4}, \\ \|\alpha\|_{\ell^2}^2 &\approx N\|A\|_{L^2}^2, & \|\alpha'\|_{\ell^2}^2 &\approx N^{-1}\|A'\|_{L^2}^2, & \|\alpha''\|_{\ell^2}^2 &\approx N^{-3}\|A''\|_{L^2}^2, \end{aligned}$$

and analogous bounds for  $\beta$  in terms of  $B$ . Here and for the remainder of the proof, “ $\approx$ ” indicates upper and lower bounds up to constants that are independent of  $\kappa, N$ .

With these definitions and derived properties we obtain (after some work) that

$$\begin{aligned} \langle K_0 u, u \rangle &= -\beta'_0 \|\alpha'\|_{\ell^2}^2 \approx -N^{-2}, \\ \langle S u, u \rangle &\approx |\beta_0|^2 \|\alpha''\|_{\ell^2}^2 + |\beta'_0|^2 \|\alpha'\|_{\ell^2}^2 \approx N^{-3}, \\ \|D u\|_{\ell^2(\Lambda)}^2 &\approx \|\alpha'\|_{\ell^2}^2 \|\beta\|_{\ell^2}^2 + \|\alpha\|_{\ell^2}^2 \|\beta'\|_{\ell^2}^2 \approx 1, \end{aligned}$$

that is,

$$\lambda_\kappa \leq \frac{\langle K_\kappa u, u \rangle}{\|D u\|_{\ell^2}^2} \leq -C_1 N^{-2} + C_2 \kappa N^{-3},$$

where  $C_1, C_2 > 0$  depend on  $A, B$  but are independent of  $\kappa$  and of  $N$  (provided  $N \geq N_0$ ).

If  $\kappa = \frac{2C_1}{3C_2} N_0 =: \kappa_0$ , choosing  $N = N_0$ , we obtain  $\lambda(\kappa) \leq -\frac{C_1}{3} N_0^{-2}$ .

For  $\kappa > \kappa_0$ , let  $N = \frac{3C_2}{2C_1} \kappa$ ; then  $N \geq N_0$ , and this implies  $\lambda_\kappa \leq -\frac{4}{27} C_1^3 C_2^{-2} \kappa^{-2}$ . This completes the proof.  $\square$

We can deduce the following instability result. Ignoring the (nontrivial) technical conditions, the result can be read as follows: *if the error in the coefficients  $\tilde{c}_1^{(m)}$  does not cancel at a critical strain  $\mathbf{G}$  (where  $H_{\mathbf{G}}^{\mathbf{a}}$  becomes unstable), then the QNL method will necessarily predict a reduced critical strain with an  $O(1)$  error. That is, the critical deformation  $\mathbf{G}$  cannot be predicted with arbitrarily high accuracy by the QNL method.* See section 2.3.1 for further discussion of this issue.

**COROLLARY 7.7.** *Consider the hexagonally symmetric case (6.4) with  $\alpha_2 = \alpha_3 = 0$ . Suppose, moreover, that*

- (i)  $\gamma(H_0^{\mathbf{a}}) = 0$ , and
- (ii)  $\tilde{c}_1^{(1)}(0) - \tilde{c}_1^{(-1)}(0) \neq 0$ .

*Then,  $\gamma(H_0^{\text{qnl}}) < 0$ .*

*In particular,  $\gamma(H_{\mathbf{G}}^{\text{qnl}}) < 0$  for sufficiently small  $|\mathbf{G}|$ .*

*Proof.* The symmetry assumptions and (i) imply that  $H_0^{\mathbf{a}} = H_0^{\mathbf{c}} = 0$ . Therefore, applying (7.11) we obtain that

$$\langle H_0^{\text{qnl}} u, u \rangle \leq 2(\tilde{c}_1^{(1)} - \tilde{c}_1^{(-1)}) \langle K_0 u, u \rangle + \kappa \langle S u, u \rangle$$

for some  $\kappa > 0$ . Lemma 7.6 implies that  $\gamma(H_0^{\text{qnl}}) < 0$ .  $\square$

**Remark 7.8.** 1. In the above corollary, (i) is an assumption on  $V$ , whereas (ii) is the assumption on an a/c scheme. We showed in section 7.4 that (ii) is generically satisfied.

2. Our numerical investigations (sections 8.1 and 8.2) indicate that similar results hold for more general  $V$  and replacing  $F = 0$  with general  $F$ , in particular dropping significantly simplifying condition  $\alpha_2 = \alpha_3 = 0$ . It does not, however, appear straightforward to extend our analysis.

**7.4. Stabilizing the 2D QNL method.** To conclude our analysis of the 2D case, we explore the issue of stabilization. Let  $S$  be given by (7.16); then we define the stabilized QNL energy functional

$$(7.19) \quad \mathcal{E}^{\text{stab}}(y) := \mathcal{E}^{\text{qnl}}(u) + \kappa \langle Su, u \rangle$$

for some  $\kappa \geq 0$ .

A consequence of Corollary 7.7 is that (under its technical conditions), for any fixed  $\kappa$ , if  $\gamma(H_G^{\text{a}}) = 0$ , then  $\gamma(H_G^{\text{stab}}) < 0$ , that is, the critical deformation  $G$  can still not be predicted with arbitrarily high accuracy. However, there is some hope that the error can be controlled in terms of  $\kappa$ . To that end, we first show that Lemma 7.6 is in fact sharp.

**THEOREM 7.9.** *Let  $K_\kappa$  and  $\lambda_\kappa$  be defined by (7.17); then there exist constants  $c_1, c_2 > 0$  such that*

$$(7.20) \quad -\frac{c_1}{(\kappa + 1)^2} \leq \lambda_\kappa \leq -\frac{c_2}{(\kappa + 1)^2} \quad \forall \kappa \geq 0.$$

*Proof.* The upper bound has already been established in Lemma 7.6, and hence we only have to show that it is sharp. For  $\kappa \leq 1$ , the lower bound is obvious, and hence we assume that  $\kappa > 1$ .

We first (crudely) estimate

$$\begin{aligned} \langle K_\kappa u, u \rangle &\geq \sum_{\xi \in \Lambda^{(0)}} \left( D_2 D_1 u(\xi) D_1 u(\xi) + \kappa \sum_{i=1}^6 |D_i D_1 u(\xi)|^2 \right) \\ &\geq \sum_{\xi \in \Lambda^{(0)}} \left( -\frac{1}{4\kappa} |D_1 u(\xi)|^2 + \kappa |D_1^2 u(\xi)|^2 \right). \end{aligned}$$

If we can prove the trace inequality

$$(7.21) \quad \|D_1 u\|_{\ell^2(\Lambda^{(0)})}^2 \leq C_1 \left( \kappa^2 \|DD_1 u\|_{\ell^2(\Lambda^{(0)})}^2 + \kappa^{-1} \|Du\|_{\ell^2(\Lambda)}^2 \right)$$

for some constant  $C_1$ , which can equivalently be rewritten as

$$-\frac{1}{4\kappa} \|D_1 u\|_{\ell^2(\Lambda^{(0)})}^2 + \kappa \|DD_1 u\|_{\ell^2(\Lambda^{(0)})}^2 \geq -\frac{c_1}{\kappa^2} \|Du\|_{\ell^2(\Lambda)}^2,$$

then the stated result follows.

*Proof of (7.21).* It turns out that (7.21) is a consequence of the embedding  $\dot{H}^1(\mathbb{R}^2) \rightarrow \dot{H}^{1/2}(\mathbb{R})$ . To make this precise we resort to Fourier analysis. Let

$$\hat{u}(k) := \sum_{\xi_1 \in \mathbb{Z}} u(\xi_1, 0) e^{ik\xi_1};$$

then  $\hat{u}$  is a periodic smooth function on  $(-\pi, \pi)$  and the following bounds hold:

$$\begin{aligned} \|D_1 u\|_{\ell^2(\Lambda^{(0)})}^2 &\approx \int_{-\pi}^{\pi} |k|^2 |\hat{u}|^2 dk, \\ \|D_1^2 u\|_{\ell^2(\Lambda^{(0)})}^2 &\approx \int_{-\pi}^{\pi} |k|^4 |\hat{u}|^2 dk, \\ (7.22) \quad \|Du\|_{\ell^2(\Lambda)}^2 &\gtrsim \int_{-\pi}^{\pi} |k| |\hat{u}|^2 dk. \end{aligned}$$

The first two bounds are completely standard. The bound (7.22) is a discrete variant of a standard trace inequality (see [22] for a proof).

We thus deduce that to prove (7.21) it is sufficient to show that there exists  $C'_1$  such that

$$k^2 \leq C'_1(\kappa^2 k^4 + \kappa^{-1}|k|) \quad \forall k \in [-\pi, \pi].$$

But, in fact, it is easy to see that  $k^2 \leq \max(\kappa^2 k^4, \kappa^{-1}|k|)$ , and hence (7.21) follows.  $\square$

We can now refine the discussion at the beginning of the section to obtain the following result.

**COROLLARY 7.10.** *Let  $V$  have hexagonal symmetry (6.4), let  $\alpha_2 = \alpha_3 = 0$ , and let  $\tilde{c}_1^{(1)} - \tilde{c}_1^{(-1)} \neq 0$ ; then there exist constants  $c_1, c_2 > 0$  such that*

$$\gamma(H_0^a) - \frac{c_1}{\kappa^2} \leq \gamma(H_0^{\text{qnl}} + \kappa S) \leq \gamma(H_0^a) - \frac{c_2}{\kappa^2}.$$

*Proof.* The result is an immediate consequence of Theorem 7.9.  $\square$

To explain the relevance of Corollary 7.10, consider the setting of section 2.3.1 and suppose, for the sake of argument, that the result holds at the critical strain,

$$\gamma(H_{G(t_*)}^a) - \frac{c_1}{\kappa^2} \leq \gamma(H_{G(t_*)}^{\text{qnl}} + \kappa S) \leq \gamma(H_{G(t_*)}^a) - \frac{c_2}{\kappa^2}.$$

It is then easy to see that the error in the critical strain will be of the order

$$(7.23) \quad |t_*^\kappa - t_*| \approx \frac{1}{\kappa^2}.$$

Therefore, if we wish to admit at most an  $O(\varepsilon)$  error in the critical strain, then we must accordingly choose  $\kappa = O(\varepsilon^{-1/2})$ . Unfortunately, this causes a larger consistency error of the stabilized QNL method, which may again cause a feedback to cause a larger error in the critical strain. In addition, if  $\kappa \gg \|\nabla^2 V(\mathcal{FR})\|$ , then the hessian operator has increased stiffness.

Both of these effects require further investigation in future work that would also need to incorporate inhomogeneous deformations. However, we note here already that our numerical experiments in section 8 indicate that already very moderate values of  $\kappa$  lead to fairly substantial quantitative improvements in the stability of the a/c coupling, and therefore the two concerns discussed above may not be of immediate practical relevance.

## 8. Numerical tests.

**8.1. Regions of stability.** We have analytically established the instability and stabilization results for the case when only nearest-neighbor bonds interact (i.e., assuming  $\alpha_2 = \alpha_3 = 0$ ). In this subsection we will study these issues in the general hexagonally symmetric case (6.4), admitting  $\alpha_2, \alpha_3 \neq 0$ . The above analytic results cannot be readily extended to this case since  $H_F^a \neq H_F^c$ , and hence we will use a seminumeric approach.

We start with a characterization of the stability of  $H_F^a$ .

**LEMMA 8.1.**  *$H_F^a$  is stable if and only if*

$$\begin{aligned} \beta_1 &:= \alpha_0 + \alpha_1 - \alpha_2 - \alpha_3 > 0, \\ \beta_2 &:= \alpha_0 + \alpha_1 + \alpha_2 + \alpha_3 > 0, \\ \beta_3 &:= 2\alpha_0 + 2\alpha_1 + 4\alpha_2 + \alpha_3 > 0. \end{aligned}$$

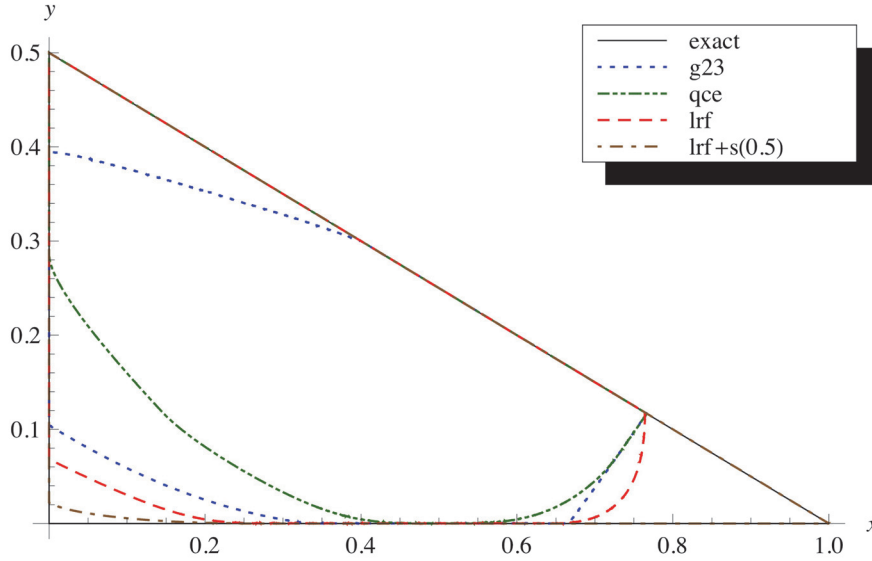


FIG. 5. Stability regions in the hexagonally symmetric case, as described in section 8.1. The exact (atomistic) stability region is the triangle, and the stability regions of the a/c methods are proper subsets of it. The last method,  $\text{lrf}+s(0.5)$ , is the stabilized coupling (8.1) with  $\kappa = 0.5$ .

*Proof.* See [22, Lemma 8.1] for the proof.  $\square$

The above lemma states that the region of stability of  $H_F^a$  is the first octant of the 3D space of parameters  $(\beta_1, \beta_2, \beta_3)$ . We will thus study the extent to which different a/c methods reproduce this exact stability region. For ease of visualization, we restrict ourselves to a hyperplane  $\beta_1 = \beta_3$  and map the stability region into a triangle

$$\{(x, y) : x > 0, y > 0, x + 2y < 1\}$$

by letting  $\beta_1 = \beta_3 = y/(1 - x - 2y)$  and  $\beta_2 = x/(1 - x - 2y)$ .

We compute the boundary of the stability region semianalytically in the following way. First, due to translational symmetry in  $\xi_1$ , it is sufficient to (formally) consider the test functions of the form  $u(\xi_1, \xi_2) = e^{i\xi_1 k_1} \bar{u}(\xi_2)$ , where  $k_1 \in (-\pi, \pi)$  and  $\bar{u} \in \mathcal{H}_0(\mathbb{Z})$ .<sup>1</sup> This reduces the problem to testing for positive definiteness of five-diagonal symmetric operators depending on  $k_1 \in (-\pi, \pi)$ . Because the operator coefficients on different diagonals for  $\xi_2 < -1$  and for  $\xi_2 > 1$  are constant, these operators can be inverted analytically. Hence, we used *Mathematica* to analytically check whether there are negative eigenvalues of these operators and used a numerical procedure of minimizing the smallest eigenvalue over  $k_1 \in (-\pi, \pi)$ .

The regions of stability of different a/c methods are plotted in Figure 5. We observe that none of the methods reproduces the exact stability region, which is consistent with the results in the case  $\alpha_2 = \alpha_3 = 0$  (cf. Corollary 7.7). Also, we see that the stabilized local reflection method

$$(8.1) \quad \langle H_F^{\text{lrf}+s(\kappa)} u, u \rangle := \langle H_F^{\text{lrf}} u, u \rangle + \kappa(|\alpha_0| + |\alpha_1| + |\alpha_2| + |\alpha_3|) \frac{1}{6} \sum_{i=1}^6 |D_i D_{i+2} u|^2$$

<sup>1</sup>To rigorously justify this step, one would need to introduce a cutoff to these test functions to ensure that they belong to  $\mathcal{H}_0(\Lambda)$ .

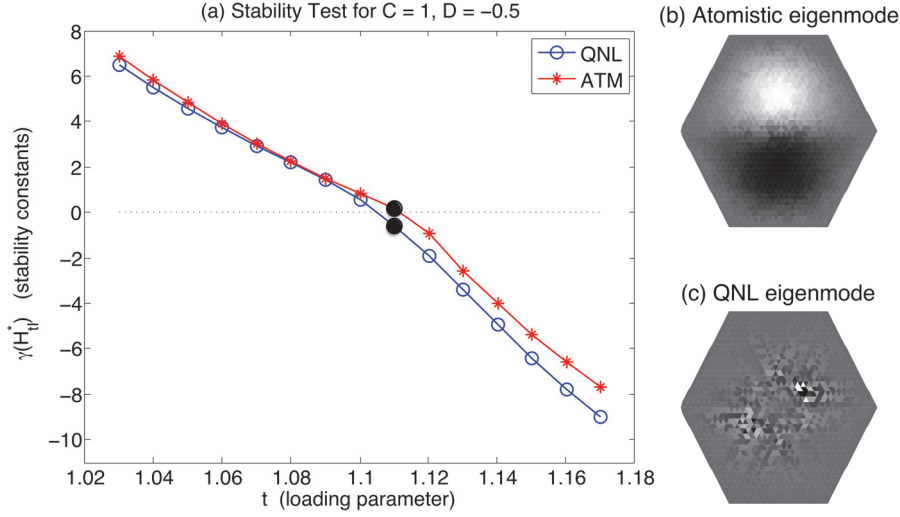


FIG. 6. Stability test for  $C = 1$ ,  $D = -0.5$ , as described in section 8.2. The black disks indicate which eigenmodes ( $u_1$ -component) are plotted in (b), (c).

with  $\kappa = 0.5$  has an improved (but not exact) stability region.

**8.2. Critical eigenmodes.** We conclude our investigations with some further numerical tests, which aim to give a preliminary assessment of the effect of the stability error on practical computations. Our experiments can only be considered preliminary since we consider only a limited class of interactions and, due to the significant computational cost involved, we do not include extensive tests on domain size dependence.

**8.2.1. Stability gap.** In these experiments we admit vectorial deformations  $y : \Lambda \rightarrow \mathbb{R}^2$ , but otherwise we use the same structure as atomistic and QNL models. The potential used in our numerical experiments is a modified EAM potential,

$$V(g) := \sum_{\rho \in \mathcal{R}} \phi(|g_\rho|) + G \left( \sum_{\rho \in \mathcal{R}} \psi(|g_\rho|) \right) + D \sum_{j=1}^6 (r_j \cdot r_{j+1} - 1/2)^2, \quad \text{where}$$

$$\phi(s) := e^{-2A(s-1)} - 2e^{-A(s-1)}, \quad \psi(s) := e^{-Bs}, \quad \text{and}$$

$$G(s) := C((s - s_0)^2 + (s - s_0)^4).$$

Throughout, we fix the parameters  $A = 3$ ,  $B = 3$ ,  $s_0 = 6e^{-0.95B}$ , but we vary  $C$  and  $D$  between experiments.

Instead of a half-space, we perform our calculations in a hexagonal domain with sidelength 18 atomic spacings and Dirichlet boundary conditions. The atomistic region is a concentric hexagon with sidelength 6 atomic spacings. We consider only the GRAC-2/3 method, which is the only force-consistent method that we know of for this setup.

Applying uniform expansion  $F(t) = tI$  as load, we obtained the results shown in Figure 6 for parameters  $C = 1$ ,  $D = -0.5$  and in Figure 7 for parameters  $C = 1$ ,  $D = 0$ .

In Figure 6(a) we observe a small but clear gap in the stability constants where they cross zero. Realistically, given the smallness of the gap, we must question whether

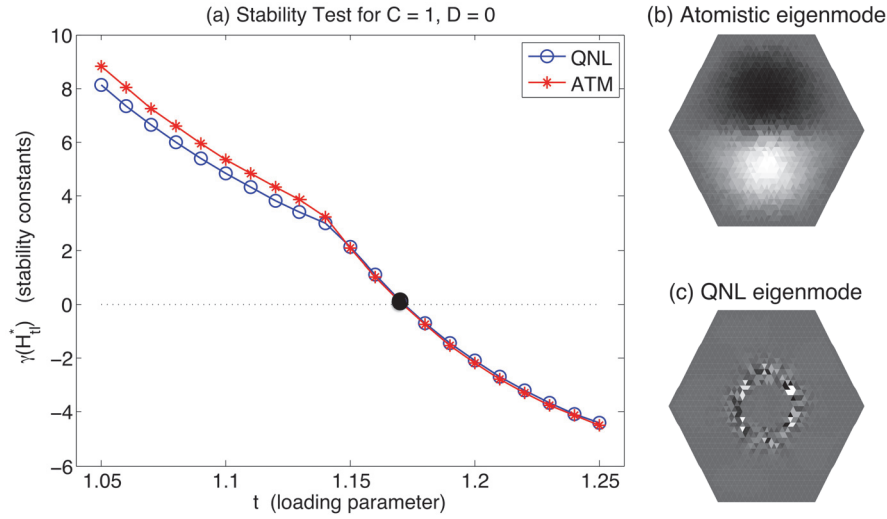


FIG. 7. Stability test for  $C = 1$ ,  $D = 0$ , as described in section 8.2. The black disks indicate which eigenmodes ( $u_1$ -component) are plotted in (b), (c).

it is genuine or a numerical error such as a domain size effect. The plots in Figures 6(b), (c) suggest that the gap is genuine since the unstable QNL eigenmode is concentrated on the interface and therefore of a different “type” than the unstable eigenmode of the atomistic model.

Interestingly, in Figure 7, we still observe the same characteristic difference in the eigenmodes, but the stability gap is essentially absent. We can only conjecture that, analytically, a gap must be present, but numerically it is too small to detect reliably. And indeed, this means that it may be of little practical relevance.

The two examples we have shown are prototypical for the entire parameter range  $C \in [-1, 1]$  and  $D \in [-1, 1]$  that we tested. Given how small the stability errors seem to be in practice (at least in these experiments), this raises the question of whether one can quantify them, instead of trying to eradicate them completely.

**8.2.2. Stabilization.** For the parameters  $C = 1$ ,  $D = -0.5$ , where we observed a visible stability gap in Figure 6, we now consider the stabilized GRAC-2/3 scheme (7.19) with  $S$  given by (7.16) and  $\kappa \geq 0$ . Repeating the numerical experiment of the previous section we obtain the results shown in Figure 8 for  $\kappa = 0.1$  and in Figure 9 for  $\kappa = 1$ .

In both experiments we observe a much smaller stability gap (for  $\kappa = 1$  no gap is visible with the naked eye), and this is accompanied by a marked change in the qualitative behavior of the critical eigenmode. In both cases, the stabilization has changed the interface supported eigenmode into a bulk eigenmode, which one might consider “smooth.” This indicates that the stability gap has closed.

For the stronger stabilization  $\kappa = 1$ , the critical QNL eigenmode is now identical to the atomistic eigenmode, while for  $\kappa = 0.1$  the QNL eigenmode has a shorter wave length. The existence of this “weaker” eigenmode explains the larger stability gap for  $\kappa = 0.1$  compared with  $\kappa = 1.0$ .

**9. Conclusion.** The stability of QNL-type a/c coupling mechanisms in dimensions greater than one remains an interesting issue. Our results in the present paper

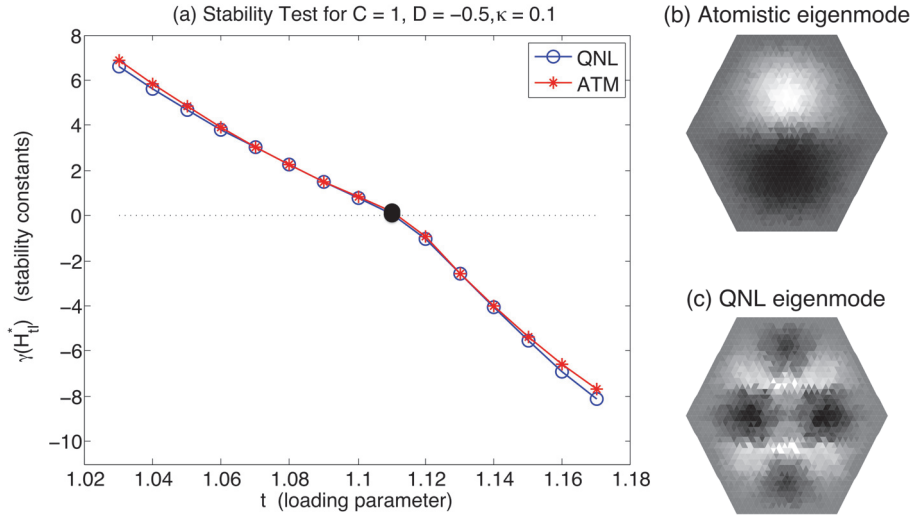


FIG. 8. Stability test for  $C = 1, D = -0.5, \kappa = 0.1$ , as described in section 8.2. The black discs indicate which eigenmodes ( $u_1$ -component) are plotted in (b), (c).

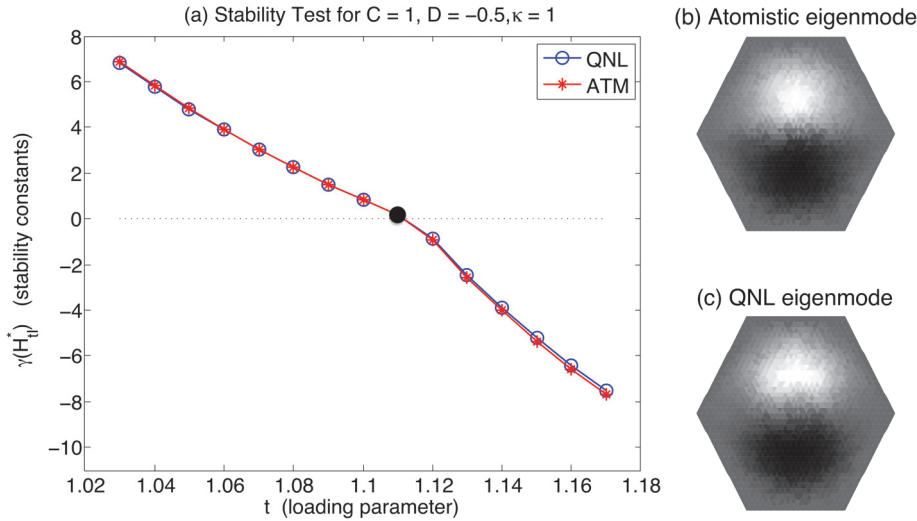


FIG. 9. Stability test for  $C = 1, D = -0.5, \kappa = 1$ , as described in section 8.2. The black discs indicate which eigenmodes ( $u_1$ -component) are plotted in (b), (c).

indicate that it is unlikely that there exists a *universally stable* variant (except in one dimension), but that suitable stabilization mechanisms must be employed.

We have proposed and analyzed a specific stabilization mechanism in a simplified setting. Our results indicate that this is a promising avenue to explore further, but that much additional work is required to establish this as a practical computational scheme.

We recall, however, that in section 8.2 we also raised the question of whether stabilization is required at all in practice since the stability errors, at least for the



class of interactions we considered there, appear to be fairly small. However, it is unclear to us at this point how one might quantify such a statement.

### Appendix.

**A.1. Details of the instability example in section 3.2.** This section describes the details of the calculation in section 3.2.

The second variation of the atomistic energy gives

$$\begin{aligned} \langle H^a u, u \rangle = & (2 - 2\alpha + 8\beta - 8\gamma + 16\delta) \sum_{\xi \in \mathbb{Z}} |D_1 u(\xi)|^2 + (\alpha - 2\beta + 18\gamma - 12\delta) \sum_{\xi \in \mathbb{Z}} |D_1^2 u(\xi)|^2 \\ & + (-8\gamma + 2\delta) \sum_{\xi \in \mathbb{Z}} |D_1^3 u(\xi)|^2 + \gamma \sum_{\xi \in \mathbb{Z}} |D_1^4 u(\xi)|^2, \end{aligned}$$

which can be written in short form as

$$\langle H^a u, u \rangle = A_1 \sum_{\xi \in \mathbb{Z}} |D_1 u(\xi)|^2 + A_2 \sum_{\xi \in \mathbb{Z}} |D_1^2 u(\xi)|^2 + A_3 \sum_{\xi \in \mathbb{Z}} |D_1^3 u(\xi)|^2 + A_4 \sum_{\xi \in \mathbb{Z}} |D_1^4 u(\xi)|^2.$$

By [10] (also Li and Luskin [11]), we have

$$\gamma(H_F^a) = \min_{0 \leq s \leq 4} A_1 + A_2 s + A_3 s^2 + A_4 s^3.$$

With the parameters in section 3.2,  $\alpha = -0.99$ ,  $\beta = 0.1$ ,  $\gamma = 0.15$ ,  $\delta = -0.2$ , we obtain that  $\gamma(H_F^a) = 0.02$ .

Similarly, the second variation of the QNL energy is

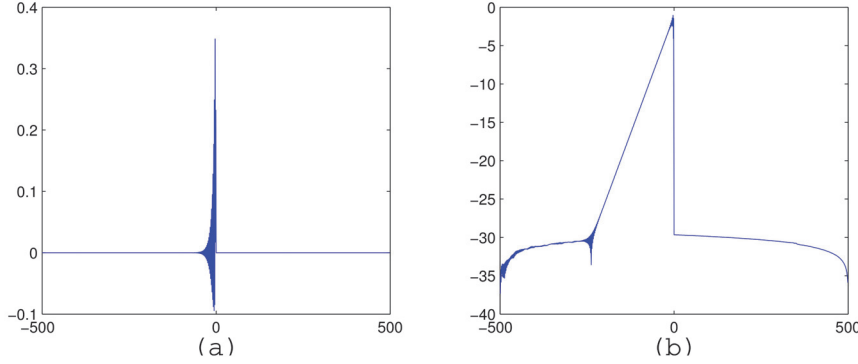
$$\begin{aligned} \langle H^{\text{qnl}} u, u \rangle = & (2 - 2\alpha + 8\beta - 8\gamma + 16\delta) \sum_{\xi \in \mathbb{Z}} |D_1 u(\xi)|^2 + (\alpha - 2\beta + 18\gamma - 12\delta) \sum_{\xi \leq -4} |D_1^2 u(\xi)|^2 \\ & + (\alpha - 2\beta + 17\gamma - 12\delta) |D_1^2 u(-3)|^2 + (\alpha - 2\beta + 15\gamma - 11\delta) |D_1^2 u(-2)|^2 \\ & + (\alpha + 6\gamma - 5\delta) |D_1^2 u(-1)|^2 + (-8\gamma + 2\delta) \sum_{\xi \leq -4} |D_1^3 u(\xi)|^2 + (-6\gamma + 2\delta) |D_1^3 u(-3)|^2 \\ & + (-2\gamma + \delta) |D_1^3 u(-2)|^2 + \gamma \sum_{\xi \leq -4} |D_1^4 u(\xi)|^2, \end{aligned}$$

which gives the explicit expression for the coefficients  $A$ ,  $B_\xi$ ,  $C_\xi$ , and  $D$  in (3.3).  $\gamma(H^{\text{qnl}})$  can be estimated by numerical calculation. For  $u$  supported in  $[-500, 500]$ , we have  $\gamma(H^{\text{qnl}}) < -0.005$ . The unstable mode is plotted in Figure 10.

**A.2. Details of the 1D QNL numerical test in section 3.3.** This section describes the details of the setup of the numerical test reported in section 3.3.

In these experiments we use  $\mathcal{R} = \{\pm 1, \pm 2\}$  and the EAM-type interaction potential

$$\begin{aligned} V(g) &:= \sum_{\rho \in \mathcal{R}} \phi(|g_\rho|) + G\left(\sum_{\rho \in \mathcal{R}} \psi(|g_\rho|)\right), \quad \text{where} \\ \phi(s) &:= e^{-2A(s-1)} - 2e^{-A(s-1)}, \\ \psi(s) &:= e^{-Bs}, \quad \text{and} \\ G(s) &:= C((s - s_0)^2 + (s - s_0)^4). \end{aligned}$$

FIG. 10. (a) *unstable mode of \$u\$ supported in \$[-500, 500]\$*; (b)  $\log(|u|)$ .

Throughout, we use the parameters  $A = 3$ ,  $B = 3$ ,  $C = 5$ , and  $s_0 = 2e^{-0.95B} + 2e^{-1.9B}$ .

Next, we redefine  $\mathcal{E}^{\text{qnl}}$  with finite atomistic and continuum regions. Fix  $K, N \in \mathbb{N}$  and a macroscopic strain  $\mathbf{F} > 0$ . Admissible deformations  $y : \mathbb{Z} \rightarrow \mathbb{R}$  are those for which  $D_1 y(\xi) > 0$  for all  $\xi$  and  $y(\xi) = \mathbf{F}\xi$  for  $|\xi| \geq N$ . Let  $\mathcal{W}_N := \{u \in \mathcal{W} \mid u(\xi) = 0 \text{ for } |\xi| \geq N\}$ ; then the admissible deformation space is  $\mathbf{F}x + \mathcal{W}_N$ .

For any admissible deformation, we then define

$$\begin{aligned} \mathcal{E}^{\text{qnl}}(y) := & \sum_{\xi=-K+2}^{K-2} [V(Dy(\xi)) - V(\mathbf{F}\mathcal{R})] \\ & + \sum_{\xi=-K}^{-K+1} [V(\tilde{D}^- y(\xi)) - V(\mathbf{F}\mathcal{R})] + \sum_{\xi=K-1}^K [V(\tilde{D}^+ y(\xi)) - V(\mathbf{F}\mathcal{R})] \\ & + \int_{-N}^{-K-1/2} [W(\nabla y) - W(\mathbf{F})] + \int_{K+1/2}^N [W(\nabla y) - W(\mathbf{F})], \end{aligned}$$

where  $\tilde{D}^+ = (D_{-2}, D_{-1}, D_1, 2D_2)$  and  $\tilde{D}^- = (2D_{-1}, D_{-1}, D_1 D_2)$ .

We will also compare the results against an atomistic model restricted to a finite domain (by simply restricting the admissible deformations as above), and against the reflection method defined in section 4, which can be analogously formulated on the finite domain.

Moreover, given parameters  $\alpha, \beta \in \mathbb{R}$ , define an external force

$$f(\xi) := \beta(1 + \xi^2)^{-(\alpha+1)/2}.$$

Finally, we discretize the continuum region using P1 finite elements. Motivated by the analysis in [17], we choose a scaling for the atomistic region size and a scaling for the mesh size, according to the decay of the external force:  $K = \lceil N^{(\alpha-1/2)/(\alpha+1/2)} \rceil$  and  $h(x) \approx (|x|/K)^{\frac{2}{3}(\alpha+1)}$ . We create the finite element mesh using the algorithm described in [17]. Let  $\mathcal{W}_h$  denote the finite element displacement space of piecewise affine functions extended by zero outside  $[-N, N]$ .

Using Newton's method, we compute a continuous path of equilibria of the energy

$$\mathcal{E}^{\text{qnl}}(y_{\mathbf{F}}) - \sum_{\xi \in \mathbb{Z}} f(\xi) \cdot y_{\mathbf{F}}(\xi), \quad y_{\mathbf{F}} \in \mathbf{F}x + \mathcal{W}_h,$$

starting with  $F = 1$  and incrementing  $F$  in small steps, using the previous step as the starting guess. Using a bisection-type approach, we can define the critical strain  $F^{\text{qn}}$  to be the smallest value of  $F$  for which  $\delta^2 \mathcal{E}^{\text{qn}}(y_F)$  ceases to be positive definite on  $\mathcal{W}_h$ . Analogously, we define the critical strains for the reflection method,  $F^{\text{rf}}$ , and for the atomistic model restricted to  $\mathcal{W}_N$ ,  $F^a$ .

The exact critical strain,  $F^*$ , is defined to be the critical strain for the unrestricted atomistic model. Since we have shown that the reflection method is universally stable, which is extended to a nonlinear deformation in [17], we compute  $F^*$  by extrapolating the computed critical  $F^{\text{rf}}$  for increasing domain sizes. The results for increasing domain sizes  $N$ , with corresponding choices of  $K$  and the finite element mesh, are displayed in section 3.3.

## REFERENCES

- [1] X. BLANC, C. LE BRIS, AND P.-L. LIONS, *From molecular models to continuum mechanics*, Arch. Ration. Mech. Anal., 164 (2002), pp. 341–381.
- [2] M. DOBSON, *There is no pointwise consistent quasicontinuum energy*, IMA J. Numer. Anal., to appear.
- [3] M. DOBSON AND M. LUSKIN, *An analysis of the effect of ghost force oscillation on quasicontinuum error*, M2AN Math. Model. Numer. Anal., 43 (2009), pp. 591–604.
- [4] M. DOBSON AND M. LUSKIN, *An optimal order error analysis of the one-dimensional quasicontinuum approximation*, SIAM J. Numer. Anal., 47 (2009), pp. 2455–2475.
- [5] M. DOBSON, M. LUSKIN, AND C. ORTNER, *Accuracy of quasicontinuum approximations near instabilities*, J. Mech. Phys. Solids, 58 (2010), pp. 1741–1757.
- [6] M. DOBSON, M. LUSKIN, AND C. ORTNER, *Sharp stability estimates for the force-based quasicontinuum approximation of homogeneous tensile deformation*, Multiscale Model. Simul., 8 (2010), pp. 782–802.
- [7] W. E, J. LU, AND J. Z. YANG, *Uniform accuracy of the quasicontinuum method*, Phys. Rev. B, 74 (2006), 214115.
- [8] W. E AND P. MING, *Cauchy-Born rule and the stability of crystalline solids: Static problems*, Arch. Ration. Mech. Anal., 183 (2007), pp. 241–297.
- [9] H. FISCHMEISTER, H. EXNER, M.-H. POECH, S. KOHLHOFF, P. GUMBSCH, S. SCHMAUDER, L. S. SIGI, AND R. SPIEGLER, *Modelling fracture processes in metals and composite materials*, Z. Metallkde, 80 (1989), pp. 839–846.
- [10] T. HUDSON AND C. ORTNER, *On the stability of Bravais lattices and their Cauchy–Born approximations*, ESAIM Math. Model. Numer. Anal., 46 (2012), pp. 81–110.
- [11] X. H. LI AND M. LUSKIN, *Analysis of the quasi-nonlocal quasicontinuum approximation of the embedded atom model*, Int. J. Multiscale Comput. Eng., 10 (2012), pp. 33–49.
- [12] X. H. LI AND M. LUSKIN, *A generalized quasi-nonlocal atomistic-to-continuum coupling method with finite range interaction*, IMA J. Numer. Anal., 32 (2012), pp. 373–393.
- [13] X. H. LI, M. LUSKIN, AND C. ORTNER, *Positive definiteness of the blended force-based quasicontinuum method*, Multiscale Model. Simul., 10 (2012), pp. 1023–1045.
- [14] X. H. LI, M. LUSKIN, C. ORTNER, AND A. V. SHAPEEV, *Theory-based benchmarking of the blended force-based quasicontinuum method*, Comput. Methods Appl. Mech. Engrg. 268 (2014), pp. 763–781.
- [15] J. LU AND P. MING, *Convergence of a force-based hybrid method for atomistic and continuum models in three dimensions*, Comm. Pure Appl. Math., 66 (2013), pp. 83–108.
- [16] J. LU AND P. MING, *Stability of a Force-Based Hybrid Method in Three Dimension with Sharp Interface*, preprint, arXiv:1212.3643v1, 2012.
- [17] M. LUSKIN AND C. ORTNER, *Atomistic-to-continuum coupling*, Acta Numer., 22 (2013), pp. 397–508.
- [18] M. MULLINS AND M. DOKAINISH, *Simulation of the (001) plane crack in  $\alpha$ -iron employing a new boundary scheme*, Phil. Mag. A, 46 (1982), pp. 771–787.
- [19] M. ORTIZ, R. PHILLIPS, AND E. B. TADMOR, *Quasicontinuum analysis of defects in solids*, Phil. Mag. A, 73 (1996), pp. 1529–1563.
- [20] C. ORTNER, *A priori and a posteriori analysis of the quasinonlocal quasicontinuum method in 1D*, Math. Comp., 80 (2011), pp. 1265–1285.
- [21] C. ORTNER, *The role of the patch test in 2D atomistic-to-continuum coupling methods*, ESAIM Math. Model. Numer. Anal., 46 (2012), pp. 1275–1319.

- [22] C. ORTNER, A. SHAPEEV, AND L. ZHANG, *(In-)stability and Stabilisation of QNL-Type Atomistic-to-Continuum Coupling Methods*, preprint, arXiv:1308.3894, 2013.
- [23] C. ORTNER AND A. V. SHAPEEV, *Analysis of an energy-based atomistic/continuum approximation of a vacancy in the 2D triangular lattice*, Math. Comp., 82 (2013), pp. 2191–2236.
- [24] C. ORTNER AND F. THEIL, *Justification of the Cauchy–Born approximation of elastodynamics*, Arch. Ration. Mech. Anal., 207 (2013), pp. 1025–1073.
- [25] C. ORTNER AND L. ZHANG, *Construction and sharp consistency estimates for atomistic/continuum coupling methods with general interfaces: A two-dimensional model problem*, SIAM J. Numer. Anal., 50 (2012), pp. 2940–2965.
- [26] A. V. SHAPEEV, *Consistent energy-based atomistic/continuum coupling for two-body potentials in one and two dimensions*, Multiscale Model. Simul., 9 (2011), pp. 905–932.
- [27] V. B. SHENOY, R. MILLER, E. B. TADMOR, D. RODNEY, R. PHILLIPS, AND M. ORTIZ, *An adaptive finite element approach to atomic-scale mechanics—the quasicontinuum method*, J. Mech. Phys. Solids, 47 (1999), pp. 611–642.
- [28] T. SHIMOKAWA, J. J. MORTENSEN, J. SCHIOTZ, AND K. W. JACOBSEN, *Matching conditions in the quasicontinuum method: Removal of the error introduced at the interface between the coarse-grained and fully atomistic region*, Phys. Rev. B, 69 (2004), 214104.
- [29] D. WALLACE, *Thermodynamics of Crystals*, Dover, New York, 1998.